

# 國立交通大學

## 電信工程學系

### 碩士論文

數種新型多天線系統分析方法

Several New Analysis Strategies of Multiple Antenna Systems

研究生：莊瑞廷

(Jui-Ting Chuang)

指導教授：陳富強 博士

(Dr. Fu-Chiarng Chen)

中華民國九十七年八月

# 數種新型多天線系統分析方法

## Several New Analysis Strategies of Multiple Antenna Systems

研究生：莊瑞廷

Student : Jui-Ting Chuang

指導教授：陳富強 博士

Advisor : Dr. Fu-Chiarng Chen



Submitted to Department of Communication Engineering  
College of Electrical Engineering and Computer Science  
National Chiao Tung University  
in partial Fulfillment of the Requirements  
for the Degree of  
Master of Science  
in  
Communication Engineering  
Aug 2008  
Hsinchu, Taiwan, Republic of China

中華民國九十七年八月

# 數種新型多天線系統分析方法

學生：莊瑞廷

指導教授：陳富強 博士

國立交通大學電信工程學系碩士班

## 摘要

在本論文中，我們研究了兩組評估多天線系統效能的電磁分析。第一項是輻射效率 (Radiation Efficiency) 的綜合分析，第二項是新型天線空間相關係數 (Antenna Spatial Correlation) 的計算方法。論文中所有的個案討論都將以偶極天線做分析基準。

首先，我們綜合分析了一個全主動反射系數 (Total Active Reflection Coefficient, TARC) 和輻射效率的表示方式。利用矩陣特徵值分解 (Eigenvalue Decomposition (EVD)) 可將 TARC 表示成天線反射功率矩陣特徵值的組合。我們利用此方法計算反射係數和輻射效率的最大值和最小值，並分析反射係數和輻射效率的特性如何隨著天線埠饋入不同相位訊號時有所改變，我們也分析不同天線匹配網路如何影響此反射係數和輻射效率。

最後我們提出兩組適用於任意大角度分佈入射角度 (Large Angular Spread Angle-of-Arrival) 的相關係數近似公式。利用此兩組公式，我們進一步計算含天線耦合效應的相關係數。基於此兩組近似公式的計算方法不僅可以有效降低計算複雜度，在精確度上也有不錯的表現。

# Several New Analysis Strategies of Multiple Antenna Systems

Student: Jui-Ting Chuang

Advisor: Dr. Fu-Chiang Chen

Department of Communication Engineering  
National Chiao Tung University

## Abstract

In the thesis, we focus on two electromagnetic analysis strategies to evaluate the performance of multiple antenna systems. The first is composite analysis of radiation efficiency. The second is a new calculation method of antenna spatial correlation. All case studies are simulated using dipole antennas.

First a composite analysis on total active reflection coefficient (TARC) and radiation efficiency are conducted. They can be described as the eigenvalues combination of antenna reflection power matrix utilizing eigenvalue decomposition (EVD). We not only evaluate the maximum and minimum value of TARC and radiation efficiency, but also their changes in characteristics when the antenna ports excite signals with different phases. Furthermore the investigations on how antenna termination networks influence TARC and radiation efficiency are also analyzed.

We further propose two new approximate antenna spatial correlation formulations which are suitable for arbitrary large angular spread angle of arrival (AoA) distribution. By using these two formulations, we further calculate spatial correlation incorporating antenna mutual coupling. Time complexity can be reduced and it still maintain good accuracy by utilizing the calculating method based on these two approximate formulations.

# Acknowledgements

I would like to express my sincere gratitude to my advisor, Dr. Fu-Chiarng Chen for his valuable suggestions, guidance, and inspiration. Without his advice, it is impossible for me to complete this research. Sincere thankfulness is also given to my elder fellow members including A-Nan, Eric, LK, A-Pen and Koo-A for their patiently discussions. Furthermore, without my fellow colleagues including JPChang, Sai, Pan, CLY and all younger lab members, it is impossible for me to keep my mind optimistic and do this research well. Moreover, I would like to thanks Dr. Yu-Min Lee and Dr. Jiun-Hwa Lin for their suggestions to this thesis.

Finally, I would like to express my deepest gratitude to my family for their concern, supports and encouragements during these years.



# Contents

<b>Chinese Abstract</b>	<b>I</b>
<b>English Abstract</b>	<b>II</b>
<b>Acknowledgements</b>	<b>III</b>
<b>Contents</b>	<b>IV</b>
<b>Figure Captions</b>	<b>VI</b>
<b>Table Captions</b>	<b>VIII</b>
<b>Acronym Glossary</b>	<b>IX</b>
<b>Chapter 1 Introduction</b>	<b>1</b>
1.1 Motivation.....	1
1.2 Purpose.....	2
1.3 Organization.....	3
<b>Chapter 2 Fundamental Theory of Multiple Antenna Systems</b>	<b>4</b>
2.1 Overview of Multiple Antenna Systems.....	5
2.2 Radiation Efficiency.....	7
2.3 Antenna Spatial Correlation.....	10
2.4 Dipole Antenna.....	12
<b>Chapter 3 Composite Analysis of Radiation Efficiency</b>	<b>14</b>
3.1 Introduction of The Eigenvalue based TARC and Radiation Efficiency.....	15
3.1.1 Multiport Antennas and Total Active Reflection Coefficient .....	15
3.1.2 Eigenvalue Representation of TARC and Radiation Efficiency.....	18
3.1.3 Simulation Results and Discussions.....	22



3.2 Composite analysis of Termination Networks on TARC and Radiation Efficiency..	29
3.2.1 50-Ohm Termination Network.....	30
3.2.2 Self-Impedance Termination Network.....	31
3.2.3 Input-Impedance Termination Network.....	33
3.2.4 Analysis and Discussion.....	34
<b>Chapter 4 New Spatial Correlation Formulations of Arbitrary AoA</b>	
<b>Scenarios</b>	<b>37</b>
4.1 2-D Approximate Spatial Correlation Formulation under Arbitrary AoA Scenarios	
.....	37
4.1.1 Spatial Correlation under Small Angular Spread AoA Scenarios.....	38
4.1.2 Spatial Correlation under Arbitrary AoA Scenarios.....	40
4.1.3 Simulation Results and Discussions.....	42
4.2 Spatial Correlation Formulation Incorporating Antenna Mutual Coupling.....	46
4.2.1 2-D Formulation Derivation Incorporating Antenna Mutual Coupling.....	46
4.2.2 3-D Formulation Derivation Incorporating Antenna Mutual Coupling.....	49
4.2.3 Simulation Results and Discussions.....	52
<b>Chapter 5 Conclusions</b>	<b>58</b>
<b>Reference</b>	<b>60</b>

# Figure Captions

Figure 2.1 The equivalent circuit of single antenna in transmitting mode.....	7
Figure 2.2 The equivalent circuit of an antenna pair in transmitting mode.....	8
Figure 2.3 (a) The $\lambda/2$ dipole and (b) the $E_\theta$ pattern in theta plane ( $\Phi=0^\circ$ ).....	13
Figure 3.1 HFSS simulation setup of dual antennas configuration.....	22
Figure 3.2 Radiation efficiency analysis using equation (2.10).....	23
Figure 3.3 EVRE analysis using equation (3.16).....	23
Figure 3.4 Three elements max. and min. radiation efficiency analysis using equation (3.18) .....	24
Figure 3.5 Four elements max. and min. radiation efficiency analysis using equation (3.18) .....	25
Figure 3.6 Five elements max. and min. radiation efficiency analysis using equation (3.18) .....	25
Figure 3.7 Maximum Efficiency Ratio for two to five elements.....	26
Figure 3.8 Dual antenna systems setup with load impedance and source impedance.....	29
Figure 3.9 Max. and min. EVRC of 50-Ohm termination network.....	30
Figure 3.10 Max. and min. EVRE of 50-Ohm termination network.....	31
Figure 3.11 Max. and min. EVRC of $Z_{11}^*$ termination network.....	32
Figure 3.12 Max. and min. EVRE of $Z_{11}^*$ termination network.....	32
Figure 3.13 Max. and min. EVRC of $Z_{in}^*$ termination network.....	33
Figure 3.14 Max. and min. EVRE of $Z_{in}^*$ termination network.....	34
Figure 4.1 AoA distribution of (a) uniform distribution over $-\Delta$ and $\Delta$ and (b) uniform-like distribution. The red dashed line and blue dashed line are the distribution curves of raised-cosine and Laplacian distributions, respectively.....	42



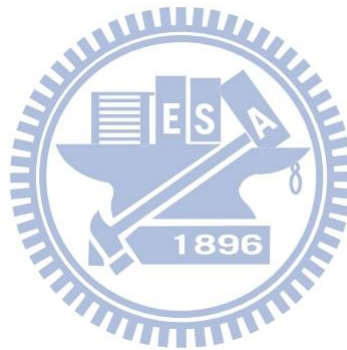
Figure 4.2 Envelope correlation of the given AoA scenario using different calculation schemes.....44

Figure 4.3 Equivalent circuit of the multiple antenna system for receiving mode.....48

Figure 4.4 2-D Envelope correlation of the given AoA scenario with and without mutual coupling effect using different calculation schemes.....53

Figure 4.5 The 3-D AoA distribution in Section 4.2.3.....55

Figure 4.6 3-D Envelope correlation of the given AoA scenario with and without mutual coupling effect using different calculation schemes.....55

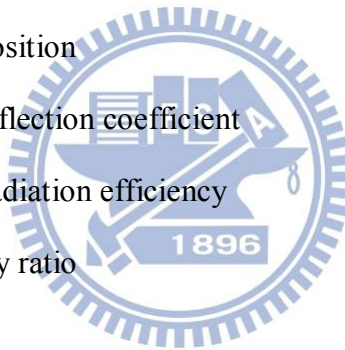


# Table Captions

TABLE 3.1 COMPARISON TABLE OF MER FOR DIFFERENT NUMBER OF ANTENNAS.....	27
TABLE 3.2 MAX. EVRE AND CORRESPONDING INPUT EXCITATION SIGNAL COMPONENTS.....	28
TABLE 3.3 MIN. EVRE AND CORRESPONDING INPUT EXCITATION SIGNAL COMPONENTS.....	28
TABLE 3.4 COMPARISON ANALYSIS TABLE FOR THREE TERMINATION NETWORKS.....	36
TABLE 4.1 EFFICIENCY COMPARISONS OF DIFFERENT SCHEMES IN FIGURE 4.2.....	45
TABLE 4.2 ACCURACY COMPARISONS OF DIFFERENT SCHEMES IN FIGURE 4.2.....	45
TABLE 4.3 ACCURACY COMPARISONS OF DIFFERENT SCHEMES IN FIGURE 4.4 (COUPLING).....	53
TABLE 4.4 EFFICIENCY COMPARISONS OF DIFFERENT SCHEMES IN FIGURE 4.6.....	56
TABLE 4.5 ACCURACY COMPARISONS OF DIFFERENT SCHEMES IN FIGURE 4.6 (COUPLING).....	56

# Acronym Glossary

2-D	two-dimensional
2G	second-generation
3-D	three-dimensional
3G	third-generation
MIMO	multiple-input multiple-output
OFDM	orthogonal frequency-division multiplexing
EVD	eigenvalue decomposition
EVRC	eigenvalue based reflection coefficient
EVRE	eigenvalue based radiation efficiency
MER	maximum efficiency ratio
EM	electromagnetic
AoA	angle-of-arrival
NLOS	non line-of-sight
PDF	probability distribution function
TARC	total active reflection coefficient
UWB	ultra-wideband
WiMAX	worldwide interoperability for microwave access
WLAN	wireless local area network
XPR	cross polarization ratio



# Chapter 1

## Introduction

In recent years, there is a great progress of wireless communication technologies which have great contributions on the whole communication industry. Wireless communication actually has changed the way we live. Standards such as the second-generation (2G) mobile communication, bluetooth and wireless local area network (WLAN) have been widely implemented since a decade ago. Moreover, some technologies like the third-generation (3G) systems, ultra-wideband (UWB), and worldwide interoperability for microwave access (WiMAX) have been suggested recently. Such these new technologies blossom on the standard platform of the wireless communication. Telecom and datacom have come to aim at higher transmission speed and lower transmission error. Mainly owing to the variety of the wireless standards, it has become an essential issue to make the best use of the limited frequency spectrum efficiently and achieve high performance on the whole communication system.

### 1.1 Motivation

The concept of multiple antenna technology has offered a solution scheme which can reach the goal of high-quality communications. From a theoretical perspective, multiple antenna transmission and reception techniques are well known in communication engineering [1] and envisioned as the solution for next generation broadband communication systems. It is acknowledged for the potential benefits for increasing the coverage, capacity, and data rates of the wireless communication systems.

Incorporating multiple antenna technology into portable wireless devices means that multiple antennas are set in the limited spacing of small devices and impacts system performance. At transmitting end, antenna radiation efficiency is an important topic when referring to the performance of multiple antenna systems. Realizing multiple antenna systems at transmitting end becomes challenging because of the unavoidable mutual coupling effect between multiple antennas. Mutual coupling effect has great impact on how much power can radiate resulting from the power absorption by adjacent antenna elements without reflection.

At receiving end, the spatial propagating channel and the characteristics of antennas are considered two key factors which actually impact system performance, and antenna spatial correlation is the composite representation of these two factors for evaluating the performance of the multiple antenna system. In previous work, antenna spatial correlation is defined as the Hermitian product of the far-field patterns of two antenna elements. This kind of definition may moreover take the probability distribution function (PDF) of angle-of-arrival (AoA) into consideration for the evaluation of the antenna spatial correlation coefficient.

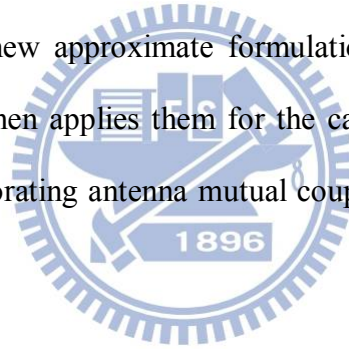
## 1.2 Purpose

In the thesis, we propose two new electromagnetic analysis strategies to evaluate the performance of multiple antenna systems. The first is a new analysis strategy of antenna radiation efficiency. This research is especially more valuable for transmitting end of communication system. The new analysis strategy can not only evaluate how the radiation efficiency may change when the antenna ports excite signals with different phases but also estimate the minimum and maximum values of radiation efficiency quickly when the number of antennas increases. The second are two new approximate formulations of antenna spatial correlation. These two new approximate formulations not only reduce computation complexity of correlation calculation but also maintain good accuracy. It can also apply for

the calculation of 2-D and 3-D parameterized spatial correlation formulation taking antenna mutual coupling effect into account.

## **1.3 Organization**

This work will be organized as follows: In Chapter 2, the overview of multiple antenna systems is introduced, and the two analysis strategies of multiple antenna systems including radiation efficiency and spatial correlation are reviewed for the further investigation in the following chapters. In Chapter 3, the newly-defined eigenvalue based reflection coefficient and eigenvalue based radiation efficiency are first proposed, and then the investigations on the impact of termination networks are further presented in the following sections of this chapter. Chapter 4 first describes two new approximate formulations of antenna spatial correlation without mutual coupling, and then applies them for the calculation of parameterized spatial correlation formulations incorporating antenna mutual coupling, both for 2-D and 3-D cases, respectively.



## **Chapter 2**

### **Fundamental Theory of Multiple Antenna**

# Systems

Wireless communication systems are becoming more important in our daily lives. The need for more data rates, wider signal coverage, larger channel capacity are several challenges in communication technologies. Multiple antenna systems have great potential in extending the signal coverage of wireless networks, increasing channel capacity, and reaching high information throughput by exploiting the spatial domain. In this chapter, we will first review the multiple antenna systems and especially focus on the detailed classification of different multiple antenna system schemes. Based on these classifications of multiple antenna systems, we further introduce two parameters which have great importance on the performance judgments of multiple antenna systems. The first one is the antenna radiation efficiency where the general definitions of single antenna and dual antennas cases will be discussed and shown why it plays an important role in multiple antenna systems. The second parameter is the antenna spatial correlation where we will review several definitions of antenna spatial correlations. Finally, because the studies we provide in the whole thesis are simulated using dipole antenna, the theory of dipole antenna is briefly introduced as well.

## 2.1 Overview of Multiple Antenna Systems

The multiple antenna technologies have been researched and developed for more than a decade which is considered substantially beneficial for the wireless communication systems. Multiple antenna systems have been implemented by several strategies, and we will introduce all of them briefly and summarize their benefits respectively as follow:

- Beamforming: Beamforming strategies originate from phased array system. The total radiation pattern of the phased antenna array system can be controlled by feeding signals with

different phase delays and antenna element spacing [2]. With a specific feeding network, the total pattern of the array can be directed to the desired direction. Recent researches focus on adaptive beamforming strategies more because it can be implemented simply by using intelligent algorithm method to steer beams toward desired signals and nulls toward interfering signals [3]. One of the adaptive beamforming method is called optimal beamforming method. Current research about this topic not only takes all electromagnetic characteristics like mutual coupling into account but also minimizes the total power radiated by the antenna array using optimization method while the response in a desired direction is maintained [4]. Beamforming offers interference rejection and antenna gain which have the equivalent effects of improving signal-interference-noise ratio (SINR) as well.

· Diversity: In telecommunications, a diversity scheme refers to a method for improving the reliability of a message signal by utilizing two or more communication channels with different characteristics. Multiple antenna systems are proposed to create the diversified channels including polarization, spatial and pattern diversity. Polarization diversity combines pairs of antenna with orthogonal polarizations. By pairing two complementary polarizations, this scheme can immunize a system from polarization mismatches that would cause signal fading. Spatial diversity systems are designed such that the signals at the different antennas of the receiver have low cross correlation with maximum gain achieved for uncorrelated signals. Antenna pattern diversity consists of two or more co-located antennas with different radiation patterns. This type of diversity makes use of directive antennas that are physically separated by some short distance. Collectively they are capable of discriminating a large portion of angle space and can provide a higher gain versus a single omnidirectional radiator.

· Spatial Multiplexing: Spatial multiplexing is a transmission technique in MIMO wireless communication to transmit independent and separately encoded data signals, so called streams, from each of the multiple transmit antennas. Therefore, the space dimension is



reused, or multiplexed, more than one time. Spatial multiplexing can reach the goal of higher data rate compared to the single-antenna communication systems and it is considered very powerful for increasing channel capacity.

The above three multiple antenna strategies can be called the family of multiple-input multiple-output (MIMO) antenna technologies and sometimes have the same characteristics of multiple antennas. Furthermore, a combination of MIMO with orthogonal frequency division multiplexing (OFDM) is promising to use the spectrum much more efficiently by spacing the channels much closer together, which is achieved by making all the carriers orthogonal to one another, preventing interference between the closely spaced carriers.

No matter what kind of MIMO technology is implemented, antenna radiation efficiency and spatial correlation have always been two very important parameters for MIMO systems. For a multi-polarization antenna system, radiation efficiency is an important issue because how much power will radiate with respect to different polarization states are concerned topics on this kind of system. Antenna spatial correlation is another issue we want to take care. For beamforming technology, we always want to design the spatial correlation as high as possible, while for diversity and spatial multiplexing techniques demand low correlation antenna setup. In the following two sections, we will review the definitions of these two parameters.

## 2.2 Radiation Efficiency

For single antenna case, the radiation efficiency is defined and computed by implementing the equivalent circuit shown in Figure 2.1[2]. We can see that input impedance is composed of real part and imaginary parts:

$$Z_A = R_A + jX_A \quad (2.1)$$

The input resistance  $R_A$  represents dissipation, which occurs in two ways. Power that leaves

the antenna and never returns (i.e., radiation) is a form of dissipation. There is also ohmic loss associated with heating on the antenna structure. The input reactance  $X_A$  represents the power stored in the near field of the antenna.

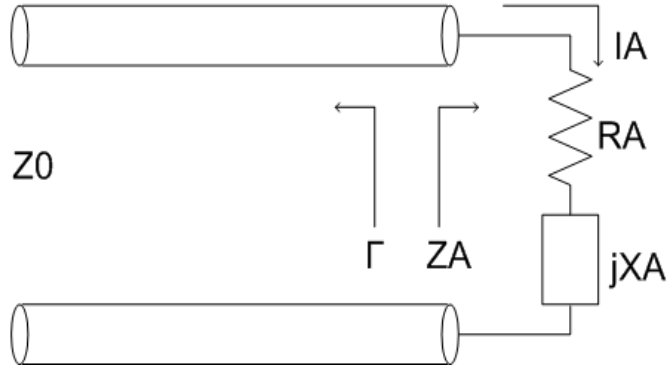


Figure 2.1 The equivalent circuit of single antenna in transmitting mode.

The average power dissipated in an antenna is:

$$P_{in} = \frac{1}{2} R_A |I_A|^2 \quad (2.2)$$

where  $I_A$  is the current at input terminals. Separating the dissipated power into radiative and ohmic losses gives:

$$P_{in} = P + P_{ohmic} \quad (2.3)$$

$$\frac{1}{2} R_A |I_A|^2 = \frac{1}{2} R_r |I_A|^2 + \frac{1}{2} R_{ohmic} |I_A|^2$$

The radiation efficiency is defined as the ratio of total radiated power to the net power accepted by the antenna, so

$$e_{oh} = \frac{P}{P_{in}} = \frac{P}{P + P_{ohmic}} = \frac{R_r}{R_r + R_{ohmic}} \quad (2.4)$$

The total radiation efficiency must take input mismatch effect into account. Therefore, the full expression of radiation efficiency on single antenna case is:

$$e_{rad1} = e_{refl1} e_{oh} \quad (2.5)$$

and

$$e_{refl1} = 1 - |\Gamma|^2 \quad \text{and} \quad \Gamma = \frac{Z_A - Z_0}{Z_A + Z_0} \quad (2.6)$$

where  $\Gamma$  is the voltage reflection coefficient and  $Z_0$  is the characteristic impedance of the

transmission line.

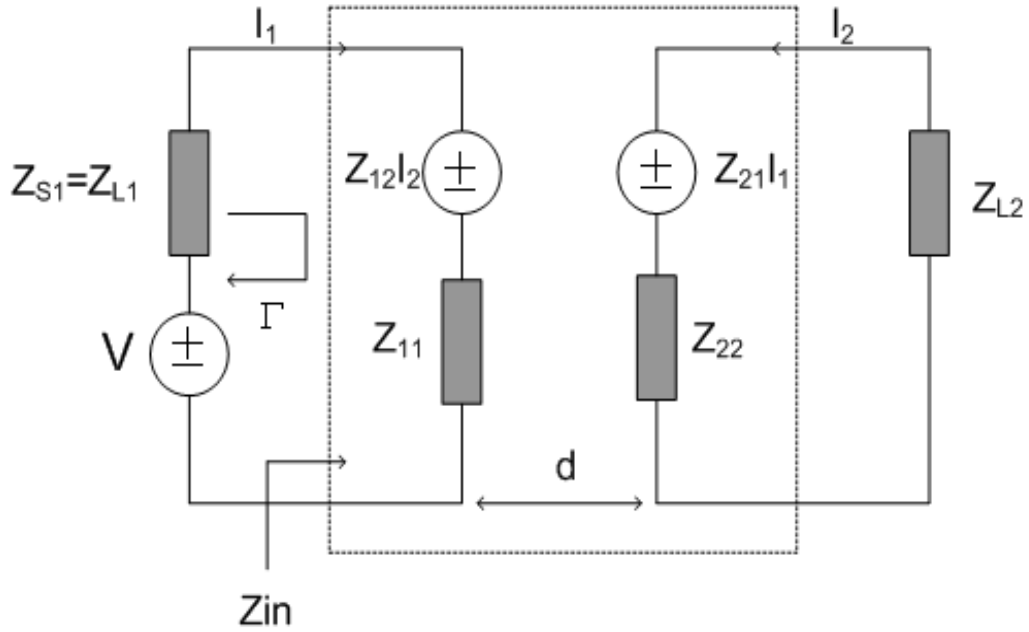


Figure 2.2 The equivalent circuit of an antenna pair in transmitting mode.

We further introduce the general definition of radiation efficiency in multiple antenna systems [5]. The radiation efficiency is defined mostly convenient in the transmit mode as the equivalent circuit shown in Figure 2.2. The voltage source  $V$  and source impedance  $Z_{S1}$  show the excitation of the antenna port 1, and the load impedance  $Z_{L2}$  is the termination at the second antenna port.  $Z_{12}$  is the mutual impedance which can describe the mutual coupling effect between two antennas. For simplicity this equivalent circuit is constructed based on the antenna pair with identical structure, which means that  $Z_{11}=Z_{22}$  and  $Z_{12}=Z_{21}$ .

The equivalent circuit in Figure 2.2 can be used to calculate the input impedance  $Z_{in}$ , which can further calculate the voltage reflection coefficient  $\Gamma_{in}$ . We can determine the input impedance  $Z_{in}$  as

$$Z_{in} = Z_{11} + \frac{Z_{12}I_2}{I_1} \quad (2.7)$$

Equation (2.7) can be further expressed using the circuit loop theory which represents the relation between  $I_1$  and  $I_2$  as:

$$I_2 = \frac{-Z_{12}}{Z_{22} + Z_{L2}} I_1 \quad (2.8)$$

As a result, we can finally determine the input impedance  $Z_{in}$  as:

$$Z_{in} = Z_{11} - \frac{Z_{12}^2}{Z_{22} + Z_{L2}} \quad (2.9)$$

The total power leaving antenna 1 is shown as  $P_{Z_{in}} = (1/2)\text{Real}\{Z_{in}\}|I_1|^2$ , and the power which will be absorbed by  $Z_{L2}$  via mutual coupling effect and cause reduction of radiation power is  $P_{Z_{L2}} = (1/2)\text{Real}\{Z_{L2}\}|I_2|^2$ . The difference between  $P_{Z_{in}}$  and  $P_{Z_{L2}}$  is called the radiation power  $P_r$ , i.e.,  $P_r = P_{Z_{in}} - P_{Z_{L2}}$ . Therefore, the radiation efficiency  $e_{rad}$  can be derived as

$$e_{rad} = e_{refl} e_{Z_{L2}} \quad (2.10)$$

where

$$e_{refl} = 1 - |\Gamma|^2 \quad \text{and} \quad \Gamma = \frac{Z_{in} - Z_{s1}}{Z_{in} + Z_{s1}} \quad (2.11)$$

$$e_{Z_{L2}} = 1 - \frac{\text{Real}\{Z_{L2}\}|I_2|^2}{\text{Real}\{Z_{in}\}|I_1|^2} \quad (2.12)$$

The radiation efficiency is the composite power efficiency representation for it includes not only the reflection caused by input mismatch of the excitation port but also the power absorption resulting from the termination at the other unexcited antenna branch.

## 2.3 Antenna Spatial Correlation

Under multiple scattering environments, signal fading is the dominant impairment existing in the wireless communication. To overcome this problem multiple antennas are typically employed to provide diversity and the performance of the multiple antennas is determined by the spatial correlation between the antennas [6]. Antenna spatial correlation was first proposed by W. C. Jakes [7]. If a signal of interest arriving at an array can be

described by the summation of plane waves arriving from azimuth angle  $\Phi$  relative to the normal between two sources a distance  $d$  apart, the spatial correlation can be determined as

$$\rho(d) = \int_{-\pi}^{\pi} \exp(j2\pi \frac{d}{\lambda} \sin(\phi)) p_{\phi}(\phi) d\phi \quad (2.13)$$

where  $\lambda$  is the wavelength and  $p_{\phi}(\Phi)$  is the azimuth angular probability distribution function. The most special case is when  $p_{\phi}(\Phi)=1/2\pi$  which is called the Clarke's model [8] and the antenna spatial correlation has a closed form well-known as the Bessel function. Based on equation (2.13), several works on spatial correlation has relied on numerical integration or series expansion to evaluate the correlation coefficient between two sources based on different azimuth angular probability distribution functions [9-11]. The author in [12] especially discussed and derived a simple formula for spatial correlation and showed that it provided a good approximation for spatial correlation of small angular spread angular distributions.

The above definitions of antenna spatial correlation only take the signal phase and the angular PDF of the incoming waves in azimuth plane. Therefore, the antenna spatial correlation including full antenna patterns and mutual coupling effect was further proposed in the literatures. There were two main formulations proposed for the antenna spatial correlation including antenna patterns and mutual coupling effect. The first is direct Hermitian product of the far-field patterns between two antenna elements. The second is parameterized correlation formulation described by scattering matrix.

• Pattern Multiplication: This is the most direct but also the most complex definition. R. G. Vaughan and J. B. Andersen proposed in [6] that the spatial correlation is given by

$$\rho_{12} = \frac{\iint_{\Omega} [F_1(\phi, \theta) \bullet F_2(\phi, \theta)] d\Omega}{\sqrt{\iint_{\Omega} |F_1(\phi, \theta)|^2 d\Omega \iint_{\Omega} |F_2(\phi, \theta)|^2 d\Omega}} \quad (2.14)$$

where  $\bullet$  denotes the Hermitian product and  $F$  means the normalize antenna pattern.

· Parameterized Formulation: The authors in [13] proposed exact representation of antenna envelope correlation in terms of scattering parameter description under the assumption of uniformly incoming waves. The approach has the advantage that it is not necessary to know the radiation pattern of the antenna system and that the explicit influence of mutual coupling and input match is revealed. The formulation is given by

$$\rho_{env} = |\rho_{12}|^2 = \frac{|S_{11}^* S_{12} + S_{21}^* S_{22}|^2}{(1 - |S_{11}|^2 - |S_{12}|^2)(1 - |S_{22}|^2 - |S_{21}|^2)} \quad (2.15)$$

Moreover, C. Waldschmidt and W. Wiesbeck further suggested a more general spatial correlation as [14]

$$\rho_{12} = \frac{R_{12}}{\sqrt{\sigma_1^2 \sigma_2^2}} \quad (2.16)$$

where

$$\begin{aligned} R_{12} &= \int_0^\pi \int_0^{2\pi} \left[ \begin{array}{l} XPR \cdot E_{\theta_1}(\phi, \theta) \cdot E_{\theta_2}(\phi, \theta) \cdot p_\theta(\phi, \theta) \\ + E_{\phi_1}(\phi, \theta) \cdot E_{\phi_2}(\phi, \theta) \cdot p_\phi(\phi, \theta) \end{array} \right] \sin \theta d\theta d\phi \quad \text{and} \\ \sigma_i^2 &= \int_0^\pi \int_0^{2\pi} \left[ \begin{array}{l} XPR \cdot |E_{\theta_i}(\phi, \theta)|^2 \cdot p_\theta(\phi, \theta) \\ + |E_{\phi_i}(\phi, \theta)|^2 \cdot p_\phi(\phi, \theta) \end{array} \right] \sin \theta d\theta d\phi \end{aligned} \quad (2.17)$$

XPR is the cross polarization ratio, E is the far-field E antenna patterns, p( $\Phi, \theta$ ) means the AoA distribution, and the subscript  $\Phi/\theta$  denotes the field polarization for both AoA distribution and antenna patterns.

Compared with the pattern multiplication and the correlation represented in S-parameter manner, both of them do not take AoA distribution of arriving signals into account. Therefore, the spatial correlation in equation (2.17) is considered the most complete and general correlation formulation so far because it takes all the possible factors into consideration.

## 2.4 Dipole Antenna

All the case studies we provide in the whole thesis are simulated using two or more half-wave dipole antennas. Therefore, the basic theory of half-wave dipole antenna is introduced in this section. The half-wave dipole antenna is the most general antenna structure, and the current distribution on the dipole usually assumes that the antenna is center-fed and the current vanishes at the end points. Moreover, to reduce the mathematical complexities, the diameter of the dipole is ideally much thinner than the wavelength of the operating frequency.

With the above assumptions, the current distribution is placed along the z-axis and for the half-sine wave current on the half-wave dipole. It is written as:

$$I(z) = I_m \sin \left[ \beta \left( \frac{\lambda}{4} - |z| \right) \right], \quad |z| \leq \frac{\lambda}{4} \quad (2.18)$$

where  $I_m$  is the maximum current occurring at the center-fed point, and  $\beta$  is the phase constant in the free space. After the cumbersome mathematical integration, the far-field  $E_\theta$  pattern is shown below:

$$E_\theta = j\eta \frac{I_m e^{-j\beta r}}{2\pi r} \left[ \frac{\cos \left( \frac{\pi}{2} \cos \theta \right)}{\sin \theta} \right] \quad (2.19)$$

In the similar manner, the total  $H_\phi$  component can be written as

$$H_\phi = \frac{E_\theta}{\eta} = j \frac{I_m e^{-j\beta r}}{2\pi r} \left[ \frac{\cos \left( \frac{\pi}{2} \cos \theta \right)}{\sin \theta} \right] \quad (2.20)$$

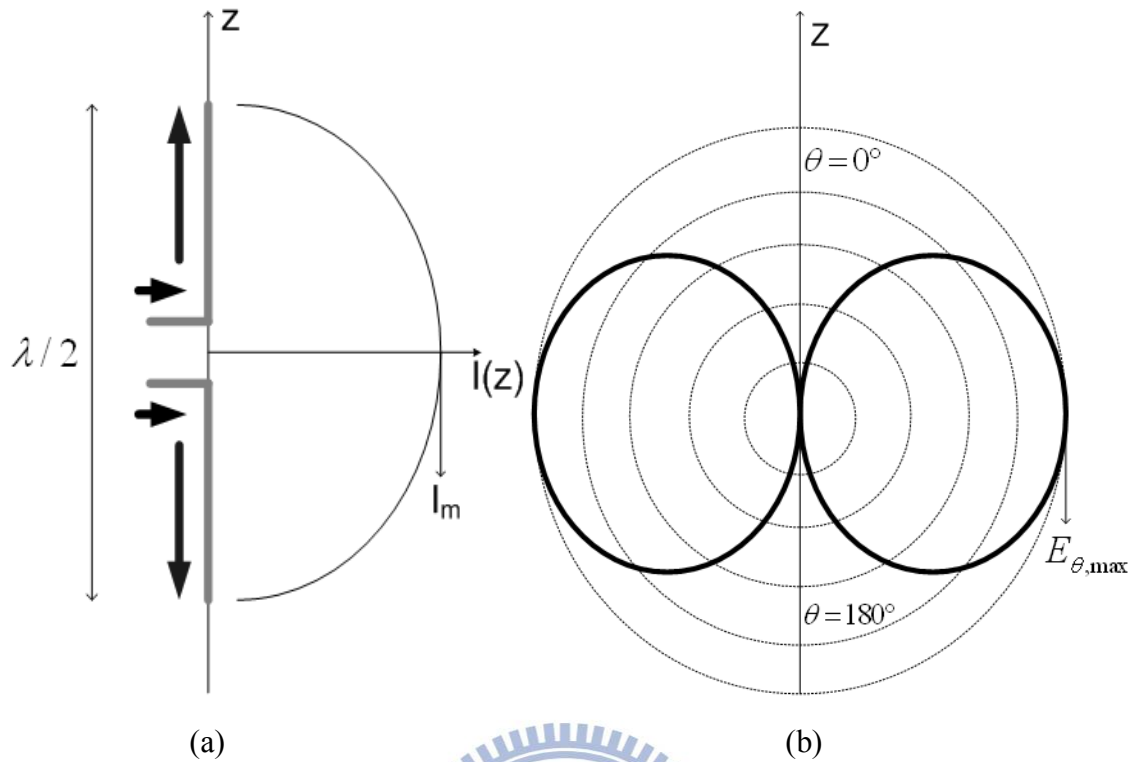


Figure 2.3 (a) The  $\lambda/2$  dipole and (b) the  $E_{\theta}$  pattern in theta plane ( $\Phi=0^\circ$ ).

The current distribution of the half-wavelength dipole and the theta-plane E-field pattern is plotted in Figure 2.3, and  $Z_{in}=73+42j$  [2]. We need to notice that we assume the diameter of the dipole is much thinner than the wavelength of the operating frequency, and there exists only  $E_{\theta}$  and  $H_{\phi}$  fields. However, in the chapter 4,  $E_{\phi}$  and  $H_{\theta}$  fields also exist in the simulation results since the diameter of the dipole is not thin enough compared to the wavelength of the operating frequency.



# Chapter 3

## Composite Analysis of Radiation Efficiency

Antenna arrays play a crucial role in wireless communication over multipath fading channels. When using multiple antenna elements for implementation on small personal communications devices, the resulting closely spaced antenna elements exhibit well-known mutual coupling, which alters radiation pattern characteristics and obviously impacts the performance of multiple antenna systems. Radiation efficiency is considered an important factor to measure the performance of multiple antenna systems including mutual coupling. In this chapter, the analysis of radiation efficiency is in transmitting mode. The general definition of radiation efficiency for dual antenna systems has been introduced in Chapter 2 and we continue this concept for the further investigations on the composite analysis of reflection coefficient and radiation efficiency. In Section 3.1, the power representation using microwave network theory and TARC are first introduced as well as the concept of [16]. The composite analysis of how different kinds of termination network impact on the reflection coefficient and radiation efficiency are conducted in Section 3.2.

### 3.1 Introduction of The Eigenvalue based TARC and Radiation Efficiency

#### 3.1.1 Multi-port Antennas and Total Active Reflection Coefficient

Assume that the scattering matrix of passive n-port antennas is  $\mathbf{S}$ . The input excitation signals  $a_i$  incident on each port  $i$  is denoted as the form of column vector  $\mathbf{a} = [a_1, a_2, \dots, a_n]^T$ , Similarly, the wave reflected from the antenna is denoted by the column vector  $\mathbf{b} = [b_1, b_2, \dots, b_n]^T$  [15][16], the relation between  $\mathbf{a}$  and  $\mathbf{b}$  is

$$\mathbf{b} = \mathbf{S}\mathbf{a} \quad (3.1)$$

The total powers incident on the n-port network is given by

$$P_{in} = \|\mathbf{a}\|^2 = \mathbf{a}^H \mathbf{a} = \sum_{i=1}^N |a_i|^2 \quad (3.2)$$

and the total power reflected from the n-port network is

$$P_{refl} = \|\mathbf{b}\|^2 = \mathbf{b}^H \mathbf{b} = \sum_{i=1}^N |b_i|^2 \quad (3.3)$$

The total input and reflected power can be represented as the summation of individual power incident on and reflected from the port  $i$ , respectively. The multiport antennas discount antenna ohmic loss for simplicity to analysis. First, we give an alternative expression to total reflected power and then we turn to calculate the radiated power. By substituting equation (3.1) into equation (3.3), the total reflected power can be written as:

$$\begin{aligned} P_{refl} &= (\mathbf{S}\mathbf{a})^H (\mathbf{S}\mathbf{a}) \\ &= \mathbf{a}^H \mathbf{S}^H \mathbf{S} \mathbf{a} \\ &= \mathbf{a}^H \mathbf{R} \mathbf{a} \end{aligned} \quad (3.4)$$

,where  $\mathbf{R}$  we call it reflection power matrix. This expression relates total power generated by excitations and the total reflected power. We now want to represent equation (3.4) in an alternative way for convenience to later analysis. Since the reflection power matrix is a Hermitian matrix, we can perform unitary similarity transformation [16] on  $\mathbf{R}$  and  $\mathbf{U}$  is unitary (i.e,  $\mathbf{U}\mathbf{U}^H = \mathbf{I}$ ) as below

$$\mathbf{R} = \mathbf{U} \mathbf{D}_s \mathbf{U}^H \quad \text{with } \mathbf{D}_s = \text{diag} \{ \lambda_{s1}, \lambda_{s2}, \dots, \lambda_{sn} \} \text{ where } \mathbf{D}_s \in R^{n \times n} \quad (3.5)$$

This transformation is also called eigenvalue decomposition (EVD). Substituting equation (3.5) into equation (3.4), an alternative representation of total reflected power is shown as

$$\begin{aligned} P_{refl} &= \mathbf{a}^H (\mathbf{U} \mathbf{D}_s \mathbf{U}^H) \mathbf{a} \\ &= (\mathbf{U}^H \mathbf{a})^H \mathbf{D}_s (\mathbf{U}^H \mathbf{a}) \\ &= \sum_{i=1}^N |q_i|^2 \lambda_{si} \end{aligned} \quad (3.6)$$

$$\text{where } \mathbf{q} = \mathbf{U}^H \mathbf{a} \quad \text{or} \quad q_i = \mathbf{u}_i^H \mathbf{a} \quad (3.7)$$

The  $i$  th column vector of matrix  $\mathbf{U}$  is denoted as  $\mathbf{U}_i$ . Note that  $\mathbf{U}_i$  is also an eigenvector of reflection power matrix.  $q_i$  can be viewed as a transformed input signal at port  $i$ . Using the fact of  $\mathbf{U} \mathbf{U}^H = \mathbf{I}$ , the total input power can also be derived as

$$\begin{aligned} P_{in} &= \mathbf{a}^H \mathbf{a} \\ &= (\mathbf{U}^H \mathbf{a})^H (\mathbf{U}^H \mathbf{a}) \\ &= \sum_{i=1}^N |q_i|^2 \end{aligned} \quad (3.8)$$

The power radiated by the antenna neglecting antenna ohmic loss is the difference between  $P_{in}$  and  $P_{refl}$ , further substitution yields as below like [16]

$$\begin{aligned} P_{rad} &= P_{in} - P_{refl} \\ &= \sum_{i=1}^N |q_i|^2 - \sum_{i=1}^N |q_i|^2 \lambda_{si} = \sum_{i=1}^N |q_i|^2 (1 - \lambda_{si}) \end{aligned} \quad (3.9)$$

The behavior of this microwave network is primarily defined by  $\lambda_{si}$ . For a lossless network,  $P_{rad}=0$  so that  $\lambda_{si}=1$  for all  $i$ . For a lossy network like multiport antennas,  $P_{rad}>0$  so that  $0 \leq \lambda_{si} < 1$  for all  $i$ . As a result, EVD for reflection power matrix facilitates analysis and provides a useful interpretation of circuits' fundamental behavior.

Now we turn to introduce the concept of TARC briefly. For a desired port excitation, the

total active reflection coefficient (TARC) [17] is defined as the square root of the available power generated from all excitations minus radiated power, divided by the available power as

$$\Gamma_{TARC} = \sqrt{\frac{P_{in} - P_{rad}}{P_{in}}} \quad (3.10)$$

For example, if an N-port antenna is excited at  $i$ th port and the other ports are connected to the matched load, the TARC can be calculated as

$$\Gamma_{TARC}^i = \sqrt{1 - p_{ri}} = \sqrt{\sum_{j=1}^N |s_{ji}|^2} \quad i = 1, \dots, N \quad (3.11)$$

For multiport excitation, the TARC is therefore in the form of

$$\Gamma_{TARC} = \frac{\sqrt{\sum_{i=1}^N |b_i|^2}}{\sqrt{\sum_{i=1}^N |a_i|^2}} \quad (3.12)$$

The TARC is a real number between zero to one. When the value of the TARC is equal to zero, all the delivered power is radiated and when it is equal to one, all the power either reflects back or goes to the other ports. This parameter is developed to describe the properties of multi-port antennas like frequency bandwidth and radiation performance, while all ports simultaneously excite signals with their own port impedances. In this manner, one is able to assess the true bandwidth of the antenna for a desired port excitation. This bandwidth information should give the multi-port antenna designer a much better understanding of the antenna bandwidth.

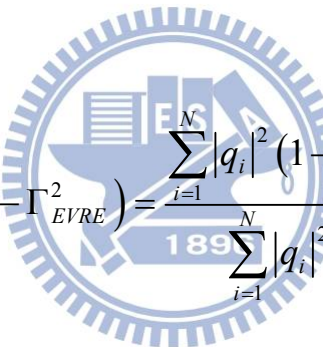
### 3.1.2 Eigenvalue Representation of TARC and Radiation Efficiency

A general definition of radiation efficiency in multiple antenna systems is introduced in

Section 2.2. Now the alternative definition of radiation efficiency is discussed in [16]. Before the derivation of radiation efficiency, we first give an alternative representation for TARC. Substituting equation (3.6) and equation (3.8) into equation (3.12), a new representation of TARC is defined as below

$$\Gamma_{TARC} = \frac{\sqrt{\sum_{i=1}^N |q_i|^2 \lambda_{si}}}{\sqrt{\sum_{i=1}^N |q_i|^2}} \quad (3.13)$$

Since this expression is based on the eigenvalues of the reflection power matrix, we redefine it as eigenvalue based reflection coefficient (EVRC) for convenient to analysis and further derive an alternative representation of radiation efficiency as below which is similar with [16] and [20]



$$e_{rad} = \left(1 - \Gamma_{EVRE}^2\right) = \frac{\sum_{i=1}^N |q_i|^2 (1 - \lambda_{si})}{\sum_{i=1}^N |q_i|^2} \quad (3.14)$$

We rename this radiation efficiency as eigenvalue based radiation efficiency (EVRE) for simplicity of the following writing. It is wondered what is the difference between equation (3.14) and equation (2.10). Equation (2.10) is considered the composite power efficiency representation. It includes not only the reflection caused by input mismatch of the excitation port but also the power absorption resulting from the termination at the other unexcited antenna branch. Based on this definition, we may find equation (2.10) is actually a special case of equation (3.14). Taking a dual-antenna system for example, equation (2.10) will let one branch of the dual antenna system excite signals and the other terminated with impedance load. While in equation (3.14), two ports of the antenna system simultaneously excite signal with their own port impedances. That exactly means if we determine the radiation efficiency

using equation (3.14) but with one branch feeding signals of zero amplitude, the analysis result will be the same as that using equation (2.10).

One of the advantages of the EVRE is it takes into account the effect when ports of the multiple antennas system are fed with signals of different phases. EVRC (TARC) is originally developed for signals with various phase delays for multi-polarization operations, and this concept can be further extended to the multiple antennas system [18]. It is well known that mutual coupling causes some portion of signal power within each element to be radiated and absorbed by the other elements. The combination of each antenna port's primary reflected signal with the coupled signals can be constructive or destructive depending on the phase of the component signals. EVRE of multiple antennas can therefore represent the effect of this constructive or destructive signal combination. Another way to show the effect of input excite signal phase difference on EVRE is based on the perspective of mathematical formulation as below: For dual antennas case and based on equation (3.13), the transformed input excitation signal is shown as

$$\mathbf{q} = \mathbf{U}^H \mathbf{a} = \begin{bmatrix} q_1(\theta) \\ q_2(\theta) \end{bmatrix} = \begin{bmatrix} u_{11}^* & u_{21}^* \\ u_{12}^* & u_{22}^* \end{bmatrix} \begin{bmatrix} 1 \\ 1e^{j\theta} \end{bmatrix} = \begin{bmatrix} u_{11}^* + u_{21}^* e^{j\theta} \\ u_{22}^* e^{j\theta} + u_{12}^* \end{bmatrix} \quad (3.15)$$

, where  $\theta$  is the phase difference of input excitation signals and the more explicit EVRC and EVRE are shown as

$$\Gamma_{EVRC}(\theta) = \frac{\sqrt{|u_{11}^* + u_{21}^* e^{j\theta}|^2 \lambda_{s1} + |u_{22}^* e^{j\theta} + u_{12}^*|^2 \lambda_{s2}}}{\sqrt{|u_{11}^* + u_{21}^* e^{j\theta}|^2 + |u_{22}^* e^{j\theta} + u_{12}^*|^2}} \quad (3.16)$$

$$\text{and } e_{rad}(\theta) = \frac{|u_{11}^* + u_{21}^* e^{j\theta}|^2 (1 - \lambda_{s1}) + |u_{22}^* e^{j\theta} + u_{12}^*|^2 (1 - \lambda_{s2})}{|u_{11}^* + u_{21}^* e^{j\theta}|^2 + |u_{22}^* e^{j\theta} + u_{12}^*|^2}$$

As a result, it can be obviously viewed from equation (3.16) that EVRC and EVRE are indeed a function of input excitation signal phase difference.

The most important advantage of EVRC and EVRE are that they provide a simple way to estimate the minimum and maximum values of reflection coefficient and radiation efficiency quickly, no matter how many number of antennas will be gauged [16]. These advantages are revealed by further deriving equation (3.13) as an inequality and it is shown below

$$\sqrt{\lambda_{s\min}} \leq \frac{\sqrt{\sum_{i=1}^N |q_i|^2 \lambda_{si}}}{\sqrt{\sum_{i=1}^N |q_i|^2}} \leq \sqrt{\lambda_{s\max}} \quad (3.17)$$

It is interesting that the minimum and maximum values of EVRC are just the square root of minimum and maximum eigenvalues of the reflection power matrix, respectively. The significances of the minimum and maximum values of EVRC are that they represent lowest reflection power and largest reflection power in the multiple antenna systems, respectively. Moreover, there exist no input excitation signal components to reach the EVRC lower than  $\sqrt{\lambda_{s\min}}$  or higher than  $\sqrt{\lambda_{s\max}}$ . Furthermore, based on equation (3.17) we can also derive an inequality for EVRE and it is shown like [16] as below:

$$1 - \lambda_{s\max} \leq e_{rad} \leq 1 - \lambda_{s\min} \quad (3.18)$$

Equation (3.18) means that the minimum or maximum EVRE occurs when maximum or minimum EVRC takes place at the same time. This phenomenon makes sense since the higher the reflection power occurs, the lower the power will radiate. Minimum and maximum values of EVRE are also considered two important quantities to judge the performance of multiple antenna systems.

What kinds of input excitation signal components will cause the maximum or minimum radiation efficiency is the another important issue. Another important advantage of EVRC and EVRE are that they both provide a convenient way to determine the input excitation signal components which may cause the best or worst case reflection coefficient and the

corresponding radiation efficiency, respectively. A mathematical proving is shown by further deriving equation (3.4) and using the result of equation (3.8) as follow: When the  $i$ th input excitation signal vector is the eigenvector of the reflection power matrix, the  $i$ th total reflection power can be determined as

$$P_{refl}^i = (\mathbf{a}^i)^H (\mathbf{R} \mathbf{a}^i) = (\mathbf{a}^i)^H (\lambda_{si} \mathbf{a}^i) = \lambda_{si} \sum_{j=1}^N |a_j^i|^2 = \lambda_{si} \sum_{j=1}^N |q_j^i|^2 \quad (3.19)$$

,where  $\mathbf{a}^i$  is the  $i$ th input excitation signal vector and  $\lambda_{si}$  is the corresponding eigenvalue. Moreover, we further derive the  $i$ th EVRC and EVRE as below [16]

$$\Gamma_{EVRC}^i = \sqrt{\frac{\lambda_{si} \sum_{j=1}^N |q_j^i|^2}{\sum_{j=1}^N |q_j^i|^2}} = \sqrt{\lambda_{si}} \quad \text{and} \quad e_{rad}^i = 1 - \lambda_{si} \quad (3.20)$$

By comparing the results between equation (3.19) and equation (3.20), we can observe that when the input excitation vector is the eigenvector of reflection power matrix, the minimum or maximum EVRC has the chance to be excited, and so does the corresponding EVRE. By utilizing unitary similarity transformation on reflection power matrix, we can easily find the corresponding input excitation signal components with the observation on the transformation matrix  $U$  when minimum or maximum EVRC takes place, and so does the corresponding EVRE. The applications and meanings of this powerful analysis strategy will be shown and discussed in the next section.

### 3.1.3 Simulation Results and Discussions



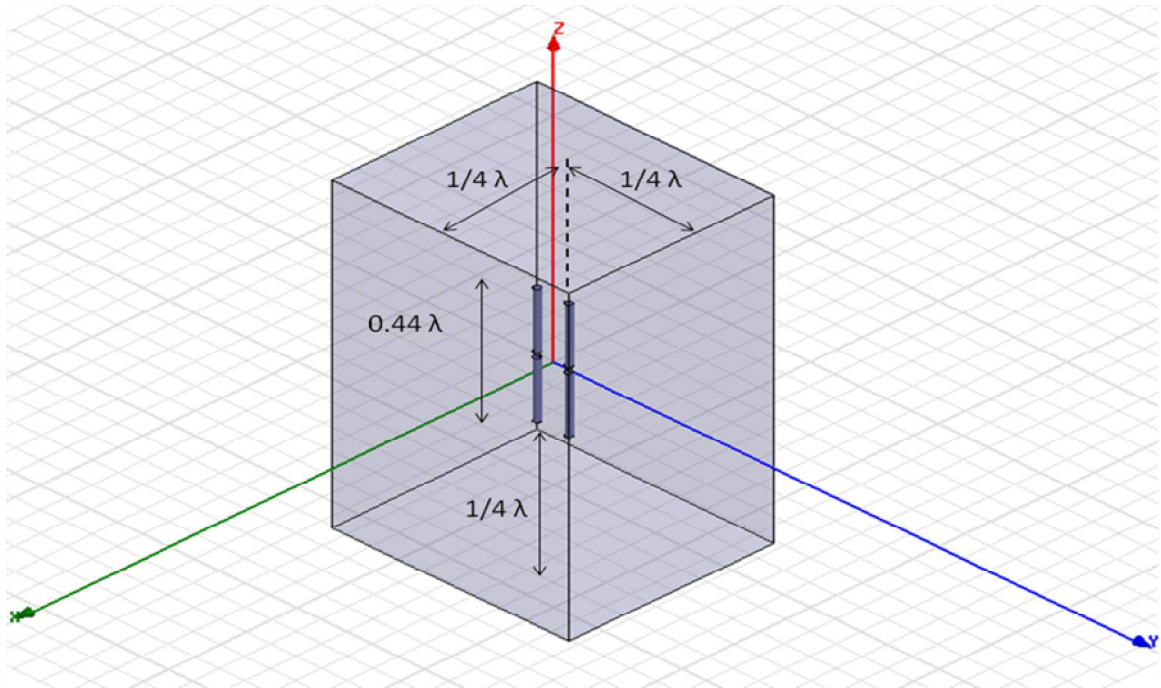


Figure 3.1 HFSS simulation setup of dual antennas configuration

Two parts of simulation results are provided in this section. First of all, we compare what is difference between conventional radiation efficiency using equation (2.10) and EVRE using equation (3.14), respectively. Secondly we offer a case study and show how the quantity of antennas affects EVRE. Moreover, we also discuss why EVRE provides powerful analysis for multiple antenna systems. We implement the case study with EM simulation software Ansoft® HFSS, while simulation programs are written in MATLAB® and run on PC with an Intel® Pentium IV 3-GHz CPU.

For convenience, the simulation environment is set with multiple dipole antennas. Figure (3.1) depicts the geometry for dual antennas. For the number of antennas is more than two, the setup of multiple antennas follows the same way as Figure (3.1), which is in symmetrical and parallel configuration. The radius of the dipole antenna is  $\lambda/100$  and the dipole length is tuned at  $0.44\lambda$  in order to make the dipole antenna resonant at the desired central frequency. In this work the central frequency is 2.45 GHz and the port impedance is set to be 50 Ohm.

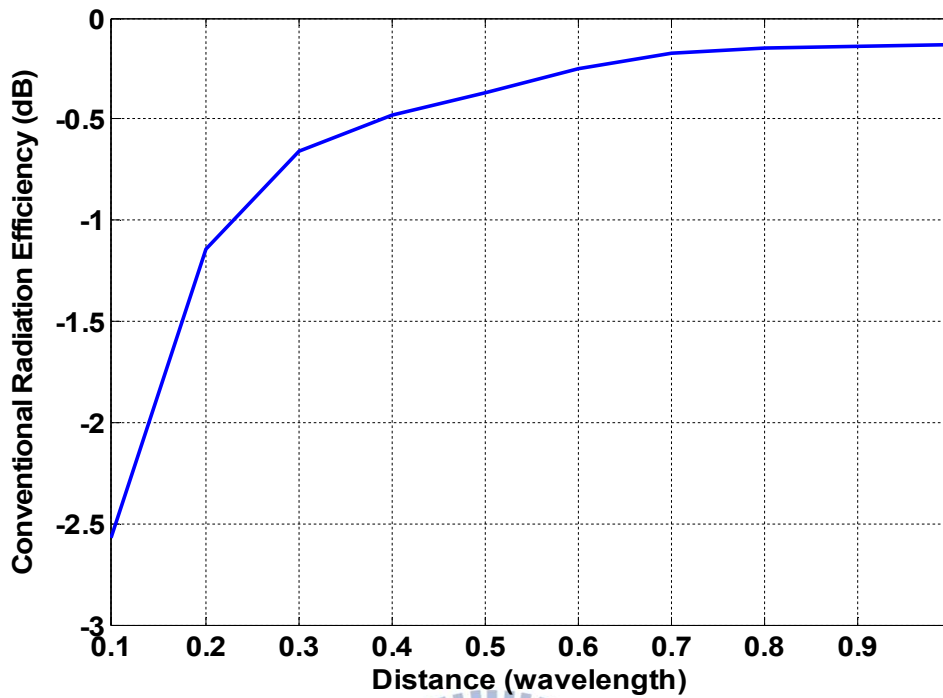


Figure 3.2 Conventional radiation efficiency analysis using equation (2.10).

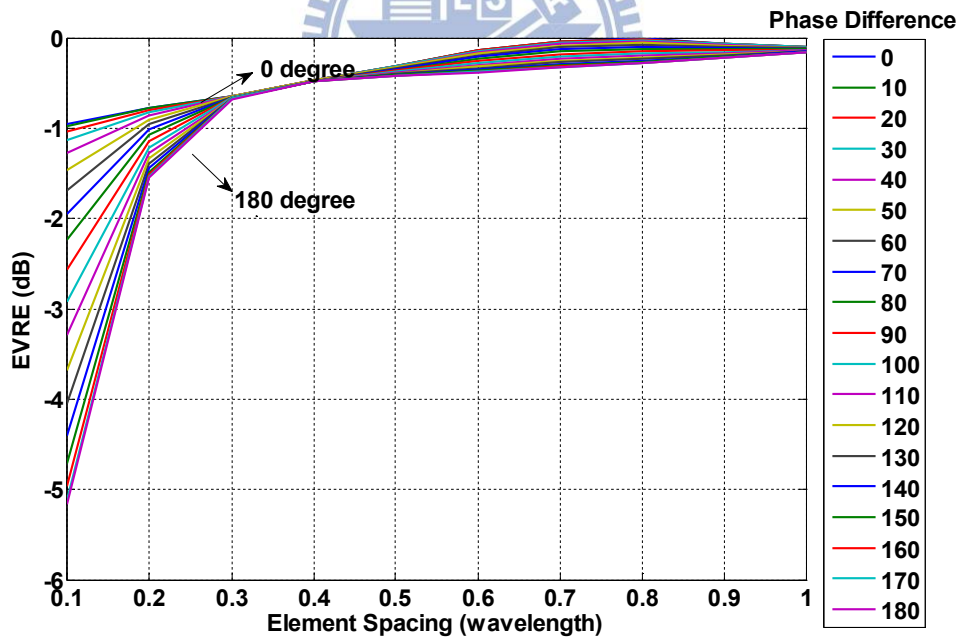


Figure 3.3 EVRE analysis using equation (3.14)

Figure 3.2 and Figure 3.3 represent the conventional radiation efficiency analysis using equation (2.10) and EVRE analysis using equation (3.14), respectively. We assume port 1 is excited with 0.707 amplitude signal and port 2 is excited with  $0.707 \cdot \exp(jx\pi/180^\circ)$  where

$x=\{0^\circ, 10^\circ, 20^\circ, \dots, 180^\circ\}$ . One reason we let both the amplitudes of the input signals to be 0.707 is that we want to maintain the summations of all input excitations power unity and both ports have equal power. This set up contains a range of excitations with same amplitude but different phase offset distribution. By comparing these two figures, we observe that the phase difference between two antenna elements deeply affects the radiation performance and the newly-defined EVRE has the ability to show this effect. From Figure 3.3, we can observe that the performance of EVRE gets worse when the phase difference becomes large. The best radiation performance takes place when the two input signals are in phase, while the worst performance occurs when the two excitations are out of phase.

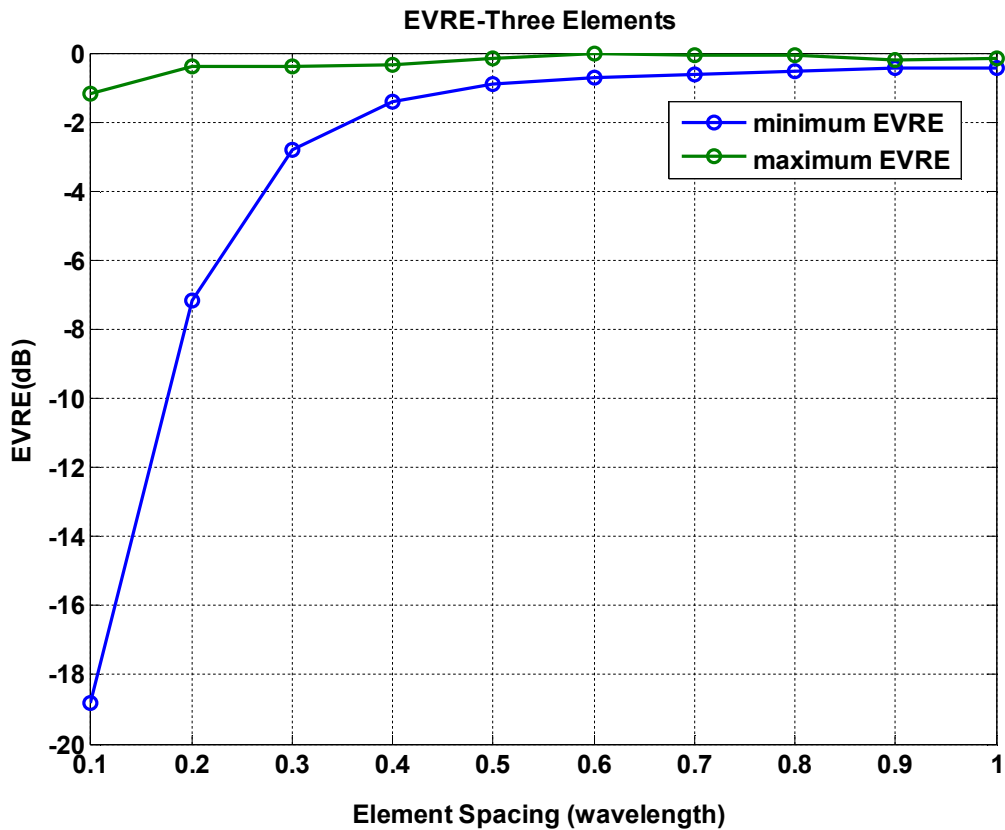


Figure 3.4 Three elements max. and min. radiation efficiency analysis using equation (3.16)

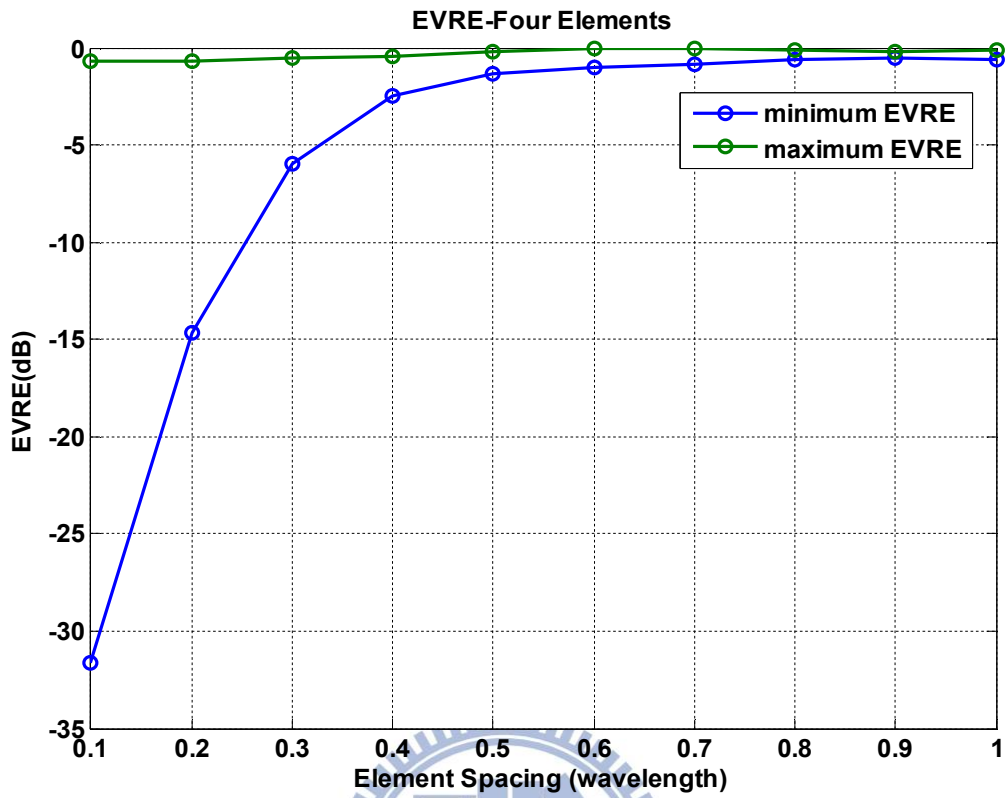


Figure 3.5 Four elements max. and min. radiation efficiency analysis using equation (3.16)

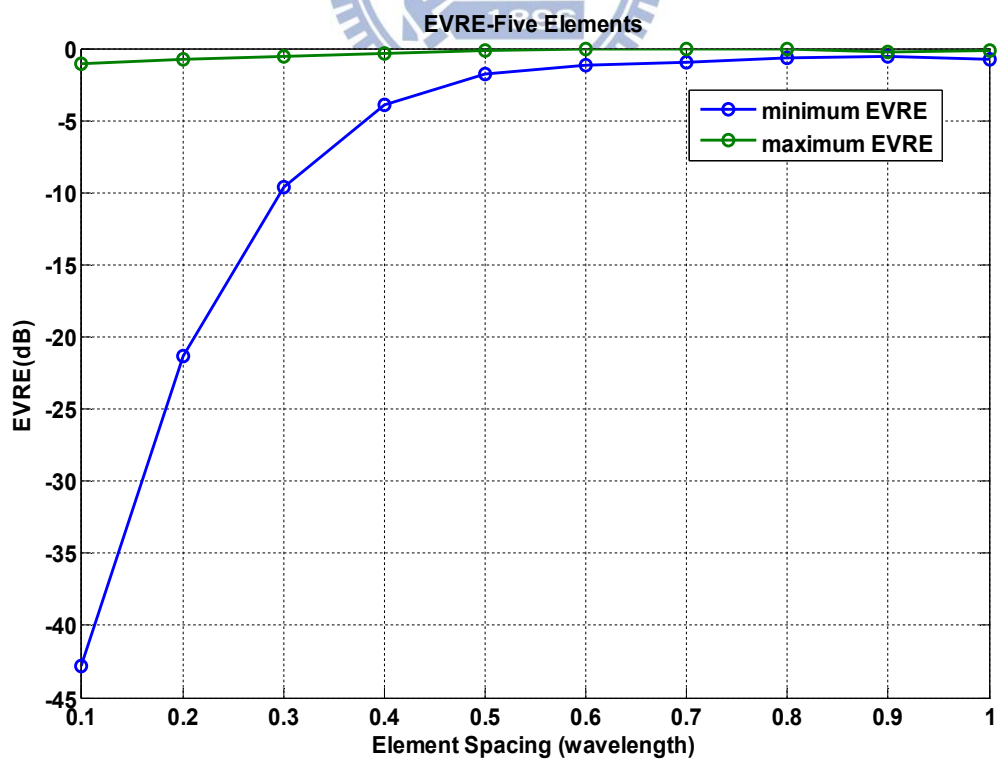


Figure 3.6 Five elements max. and min. radiation efficiency analysis using equation (3.16)

Finding the best or worst performance of EVRE for the number of multiple antennas more than two becomes cumbersome if we use the same way as dual antennas case presented before. However, it becomes easily and quickly to obtain the maximum and minimum values of EVRE by utilizing equation (3.16), which can be easily derived from equation (3.14) or equation (3.15). Figure 3.4 to Figure 3.6 represent the results when the number of antenna becomes three to five. We first define a parameter called Maximum Efficiency Ratio (MER), which means the ratio in dB between the maximum and the minimum EVRE to facilitate analysis. An observation from Figure 3.4 to Figure 3.6 is if the antenna elements are in close proximity, the radiation efficiency will have larger MER which means the performance may be very good or very bad at a given close antenna element spacing. The MER will become smaller as the antenna element spacing increase, which means the performance becomes better and more stable as mutual coupling between antenna elements is less strong.

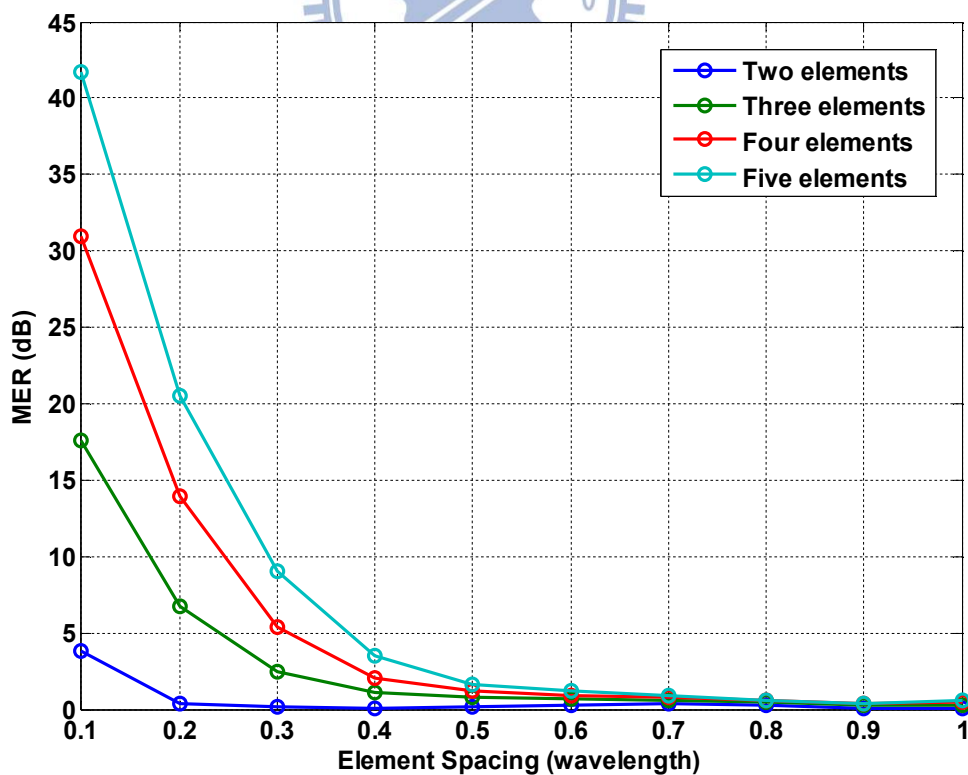


Figure 3.7 Maximum Efficiency Ratio for two to five elements

As the number of antenna elements increases, the maximum EVRE maintains almost the same while the minimum EVRE decreases a lot at fixed element spacing. The MER therefore becomes larger as shown in Figure 3.7 and a comparison table is shown as in TABLE 3.1. Take  $0.1\lambda$  inter-element spacing as an example, the MER increases from 3.8 dB to 42 dB while the number of antenna increases from two to five which show the same tendency as the diagram depicted in [16]. The reason for this fact may due to higher mutual coupling and it results in more input mismatch effects at the central elements of these symmetrical multiple antenna sets when the number of antennas increase. As a result, there exists a set of input excitation signal components which cause the minimum EVRE worse.

TABLE 3.1 COMPARISON TABLE OF MER FOR DIFFERENT NUMBER OF ANTENNAS.

Antenna Number	Maximum Efficiency Ratio(MER) at $0.1 \lambda$
2	3.83 dB
3	17.64 dB
4	30.93 dB
5	41.75 dB

Finding the corresponding input excitation signal components when the best or the worst performance of multiple antenna systems (Maximum EVRE or Minimum EVRE) takes place by trying an error is nearly impossible when the number of antennas is more than two. By utilizing the eigenvalue decomposition shown in equation (3.17) to equation (3.19), these input excitation signal components are easily determined simply by solving the eigenvectors of reflection power matrix. The results are shown in Table 3.2 and Table 3.3 taking

0.1  $\lambda$  inter-element spacing as an example. One thing to be mentioned is that the summation of the power from every port is equal to unity.

TABLE 3.2 MAX. EVRE AND CORRESPONDING INPUT EXCITATION SIGNAL COMPONENTS.

Antenna Number	Max. EVRE at 0.1 $\lambda$	Input Excitation Signal Components
2	-0.96 dB	$[0.707\angle 0^\circ, 0.707\angle 0^\circ]$
3	-1.17dB	$[0.703\angle 0^\circ, 0.013\angle 86^\circ, 0.703\angle 180^\circ]$
4	-0.72dB	$[0.654\angle 180^\circ, 0.269\angle -164^\circ, 0.269\angle 16^\circ, 0.654\angle 0^\circ]$
5	-1.01dB	$[0.589\angle 180^\circ, 0.391\angle -153^\circ, 0, 0.391\angle 27^\circ, 0.589\angle 0^\circ]$

TABLE 3.3 MIN. EVRE AND CORRESPONDING INPUT EXCITATION SIGNAL COMPONENTS.

Antenna Number	Min. EVRE at 0.1 $\lambda$	Input Excitation Signal Components
2	-4.79 dB	$[0.707\angle 180^\circ, 0.707\angle 0^\circ]$
3	-18.81dB	$[0.463\angle 0^\circ, 0.756\angle -158^\circ, 0.463\angle 0^\circ]$
4	-31.65dB	$[0.275\angle 180^\circ, 0.657\angle 17^\circ, 0.651\angle -164^\circ, 0.263\angle 0^\circ]$
5	-42.76dB	$[0.155\angle 180^\circ, 0.488\angle 12^\circ, 0.69\angle -165^\circ, 0.488\angle 12^\circ, 0.155\angle 180^\circ]$

An observation from Table 3.2 is that the power and phase of the input excitation signal at each port should be properly distributed and adjusted in order to reach the best performance. However, Table 3.3 gives us information that we should avoid exciting such input excitation signal components which will cause the worst performance. The eigenvalue representations of TARC and radiation efficiency in [16] provide us a quickly way to determine the best and worst radiation efficiencies and their corresponding input excitation signal components. Based on [16] we do further analysis on its characteristics in the following chapter.

### 3.2 Composite analysis of Termination Networks on TARC and Radiation Efficiency

It has been shown that different kinds of termination networks may have great impact on conventional radiation efficiency [5]. In this section, the impact of termination networks including 50-Ohm, self-impedance and input impedance termination networks on EVRC and EVRE are investigated accordingly. A thoroughly comparisons about the performances of these three termination networks are also conducted in this section.

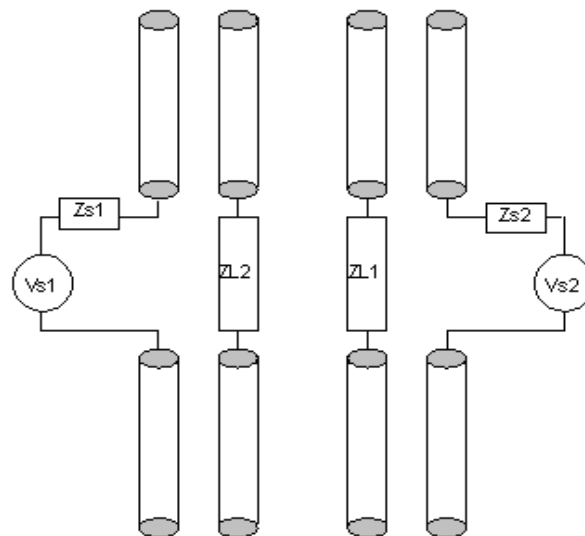


Figure 3.8 Dual antenna systems setup with load impedance and source impedance



### 3.2.1 50-Ohm Termination Network

The simulation setup is shown as in Figure 3.8 and both the antennas are identical and have the same conditions as the previous section. It means that  $Z_{L1}(=Z_{S1}$  when port 2 excitation) and  $Z_{L2}(=Z_{S2}$  when port 1 excitation).  $Z_{S1}=Z_{S2}=50$  Ohm first comes as the first case study. It is the most common topology for its wideband characteristic and easier implementation. Figure 3.9 and Figure 3.10 respectively show the maximum and minimum values of EVRC and EVRE using equation (3.15) and equation (3.16). Note that the reflection swing range here is defined as the difference between maximum and minimum EVRC, where the radiation swing range is defined as the difference between maximum and minimum EVRE.

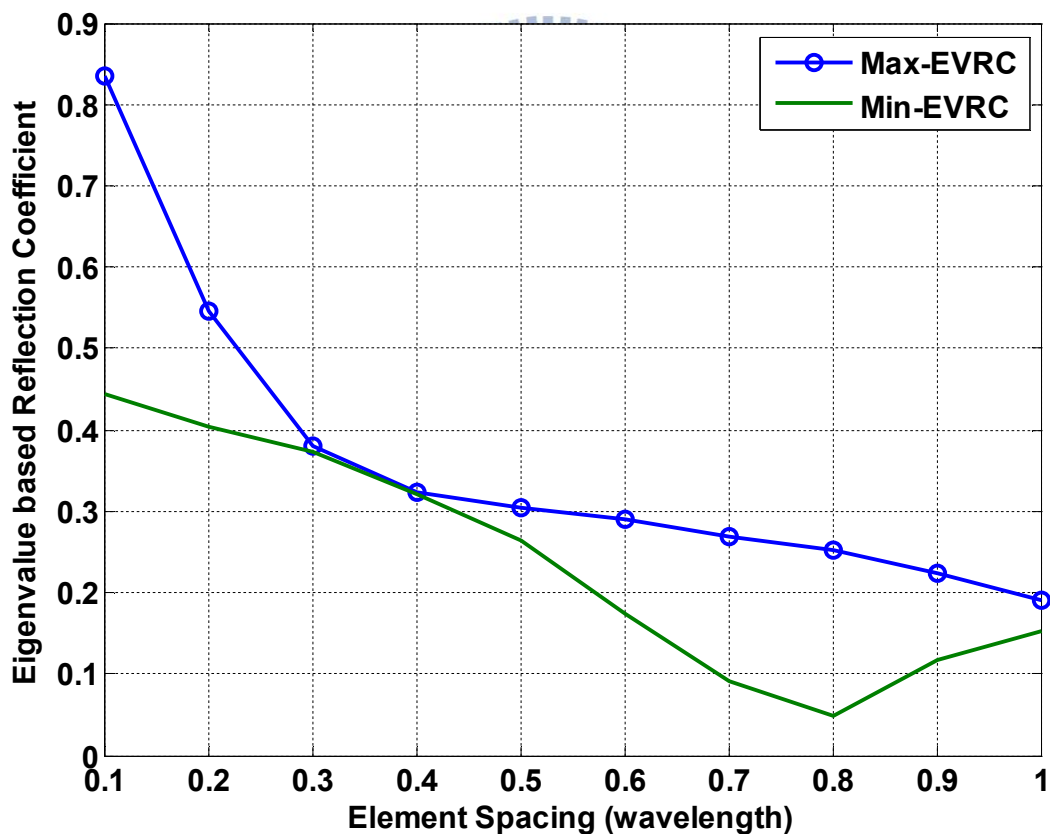


Figure 3.9 Max. and min. EVRC of 50-Ohm termination network

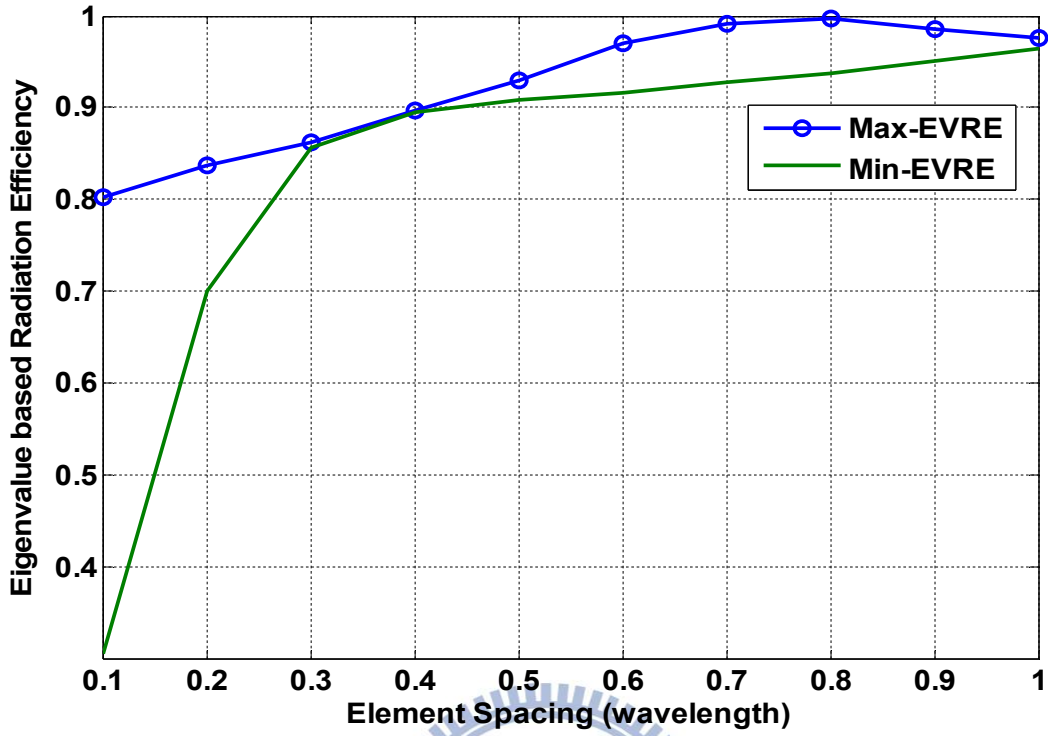


Figure 3.10 Max. and min. EVRE of 50-Ohm termination network

### 3.2.2 Self-Impedance Termination Network

The termination network such as  $Z_{S1}=Z_{S2}=Z_{11}^*$  is known as the self-impedance source matching (termination) network, which is also known as complex conjugate match and it facilitates maximum power transfer to the load when there is no mutual coupling. The goodness of the match depends on the behavior of the mutual impedance which is not taken into account. What can be mentioned in this simulation procedure is we do not need to re-simulate the dual antenna systems which use 50-Ohm port termination in the previous section to solve the new scattering matrix. However, by using the formulation as below

$$[S_{new}] = [ZZ_{port}^{-1} + U]^{-1} [ZZ_{port}^{-1} - U] \quad (3.21)$$

where  $Z$  is the impedance matrix,  $Z_{port}$  is the diagonal matrix with diagonal terms(= $Z_{S1}$  and  $Z_{S2}$ ), and  $U$  is the unitary matrix, the new scattering matrix  $S_{new}$  can thus be computed and used in the calculation of EVRC and EVRE. Figure 3.11 and Figure 3.12 respectively show

the maximum and minimum value of EVRC and EVRE using equation (3.15) and equation (3.16).

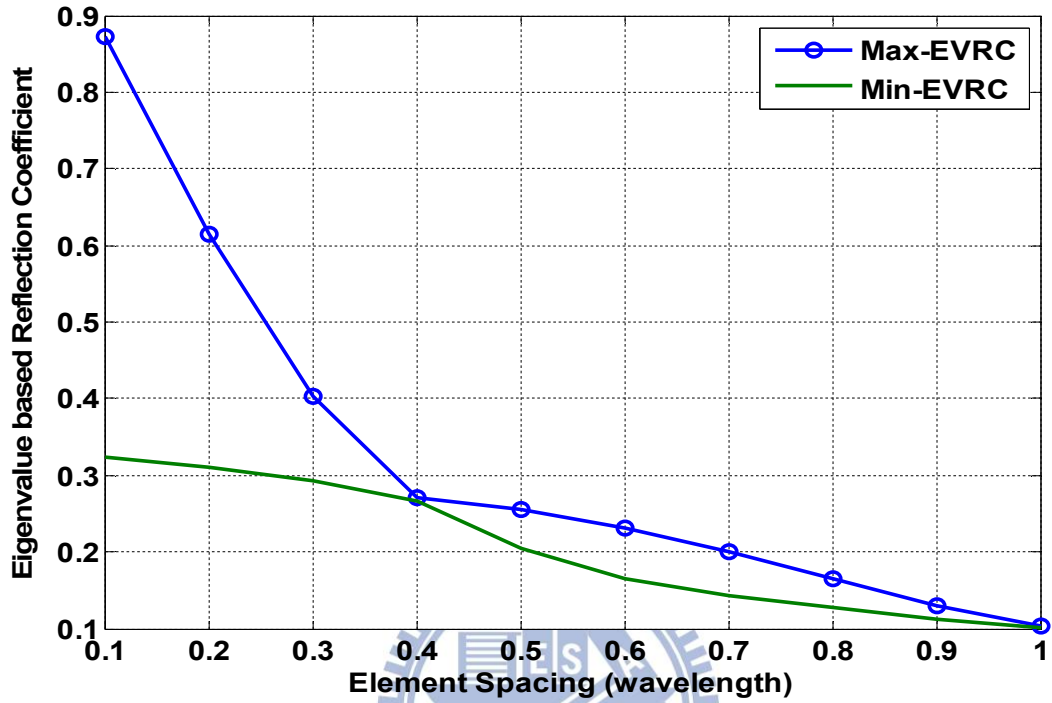


Figure 3.11 Max. and min. EVRC of  $Z_{11}^*$  termination network

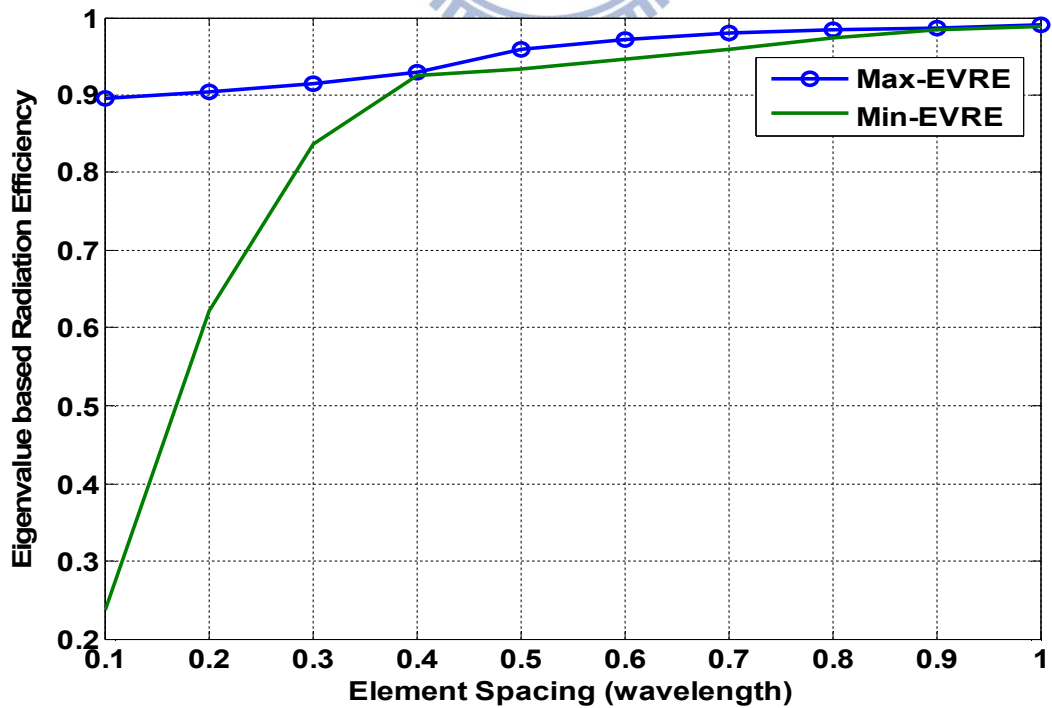


Figure 3.12 Max. and min. EVRE of  $Z_{11}^*$  termination network

### 3.2.3 Input-Impedance Termination Network

Input-impedance matching termination is considered more complete for it takes into account not only the reflection from the single antenna element but also the mutual coupling effect which results from the adjacent antenna element. It refers to maximum power transfer from the single excited source into the corresponding antenna port, which gives no consideration to power coupled into adjacent antenna. Because  $Z_{S1}$  is the function of  $Z_{L2}$  and vice versa, we may finally derive  $Z_{S1}$ , based on equation (2.9) and  $Z_{S1}=Z_{in}^*$ , as

$$Z_{S1} = \sqrt{R_{11}^2 - R_{12}^2 + X_{12}^2 - \frac{R_{12}^2 X_{12}^2}{R_{11}^2}} + j \left( \frac{R_{12} X_{12}}{R_{11}} - X_{11} \right) \quad (3.22)$$

where  $R_{11}$  and  $X_{11}$  are the real and imaginary part of self impedance,  $R_{12}$  and  $X_{12}$  are the real and imaginary part of mutual impedance. Moreover, the new scattering matrix with  $Z_{in}^*$  port termination can also be computed and used in calculation of EVRC and EVRE by equation (3.15) and equation (3.16). Figure 3.13 and Figure 3.14 respectively show the maximum and minimum value of EVRC and EVRE using equation (3.15) and equation (3.16).

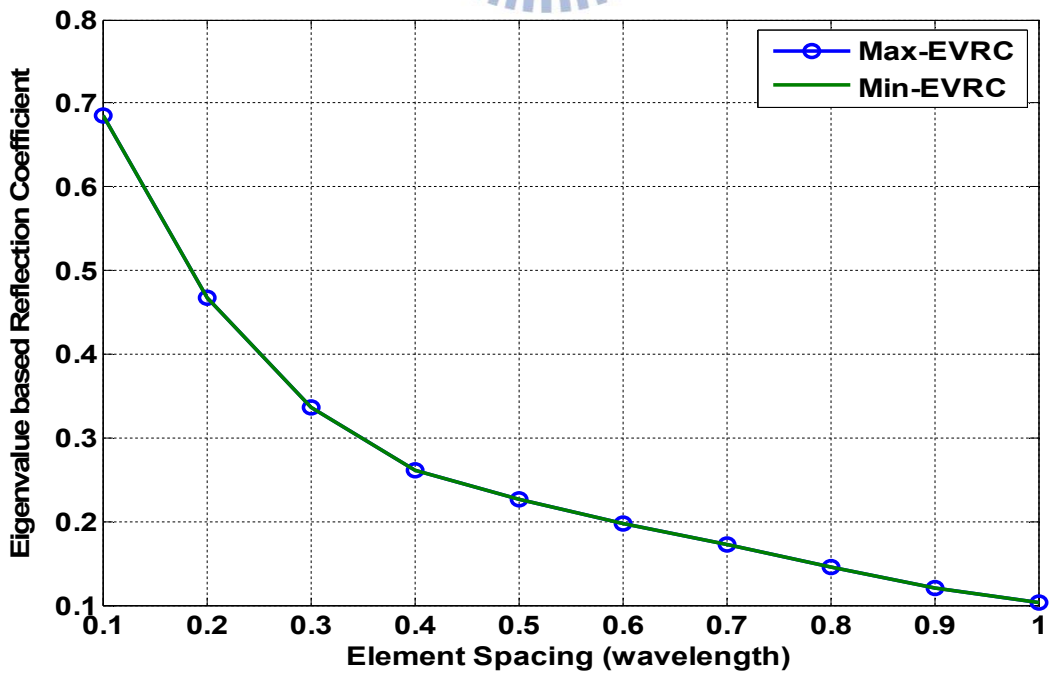


Figure 3.13 Max. and min. EVRC of  $Z_{in}^*$  termination network

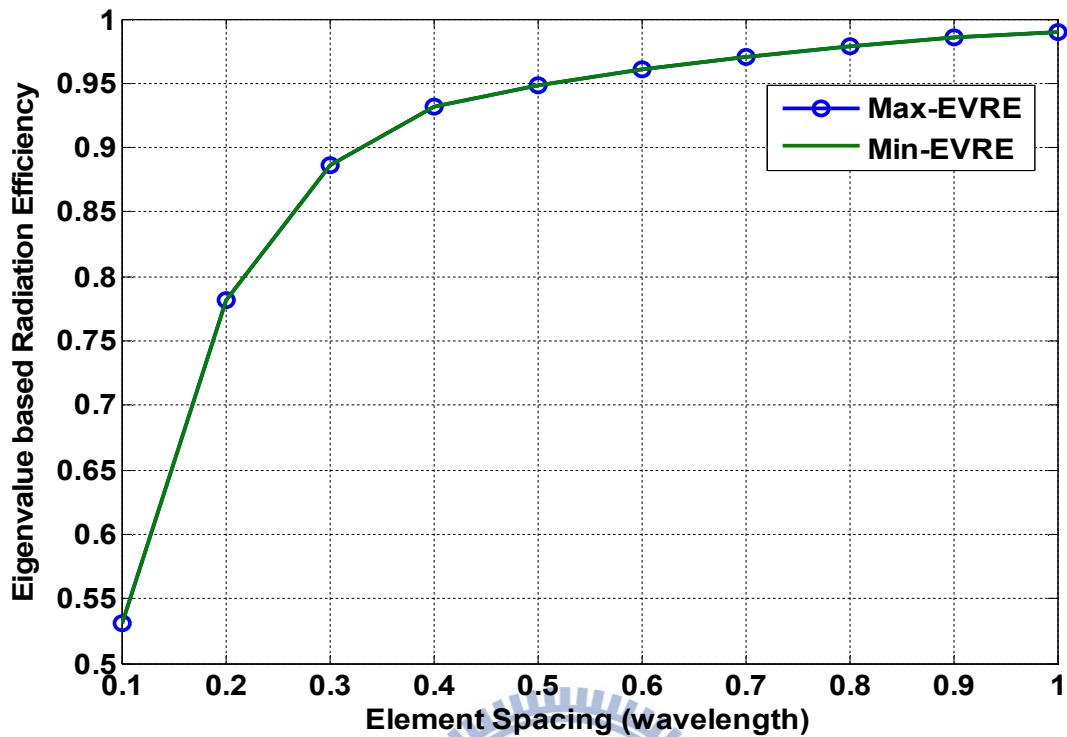


Figure 3.14 Max. and min. EVRE of  $Z_{in}^*$  termination network

### 3.2.4 Analysis and Discussion

EVRC for three termination cases are shown in Figure 3.9, Figure 3.11 and Figure 3.13. EVRE for three termination cases are shown in Figure 3.10, Figure 3.12 and Figure 3.14. For a dual antenna systems case, the input excitation signals for port1 and port 2 have equal power in order to reach the best or worst performance as shown in TABLE 3.2 and TABLE 3.3. Therefore, the radiation swing range depends only on the phase difference of two input excitation signals. Larger radiation swing range means that EVRE is more sensitive to the phase variation of input signals, and on the contrary smaller radiation swing range means that EVRE is less sensitive to the phase variation of input signals. EVRC is also an important parameter for the performance judgment of multiple antenna systems. For examples, lower or higher EVRC means higher or lower EVRE, respectively. Larger reflection swing range or

lower reflection swing range for EVRC means larger radiation swing range or lower radiation swing range for EVRE, respectively.

The largest reflection swing range of EVRC and the largest radiation swing range of EVRE happens when antenna element spacing is  $0.1 \lambda$  for the first two matching cases. For 50-Ohm case, the largest swing ranges for EVRC and EVRE are about 0.39 and 0.5, respectively. For  $Z_{11}^*$  case, the largest swing ranges for EVRC and EVRE are about 0.55 and 0.66, respectively. For  $Z_{in}^*$  case, we can observe that there exist no swing range for both EVRC and EVRE. The reason for this phenomenon results from that  $Z_{in}^*$  not only takes into account the self-impedance of the antenna but also mutual coupling effect. It will cause very low  $S_{11}$  and thus results in no swing range for both EVRC and EVRE. Furthermore, we can observe that the swing range for both EVRC and EVRE would be greatly reduced as element spacing becomes larger. It can be interpreted as when the mutual coupling effect is reduced, the EVRC and EVRE both become much less sensitive to the phase variation of input signal.

Another interesting phenomenon observed from EVRC (Figure 3.9 and Figure 3.12) and EVRE (Figure 3.10 and Figure 3.13) for the first two matching cases is that there exist some element spacings which are nearly immune from the variation of different phases. For 50-Ohm and  $Z_{11}^*$  case the first crossing points both occur at element spaces= $0.4 \lambda$ . It is an important parameter provided for the design of multiple antenna systems since we can find the best element spacing which will not be seriously impacted by the unpredictable variation of signal excitation phases between two ports. A comparison table is shown as in TABLE 3.4. From the comparison we find although the first crossing points of 50-Ohm case is at  $0.4\lambda$ , the corresponding EVRC and EVRE are 0.33 and 0.9, respectively while for  $Z_{11}^*$  case the corresponding EVRC and EVRE are about 0.27 and 0.93, respectively. It means less than 10 % of the incident power either reflects back or is absorbed by the load of the adjacent antenna element. As a result,  $0.4\lambda$  is a good candidate for the design of multiple antenna systems for

the first two matching cases. For  $Z_{in}^*$  case it can be immune from phase variation of input signals so how much power will radiate is what we may concern more. At  $0.1 \lambda$ , the EVRC and EVRE are 0.68 and 0.53, respectively. It means more than 47 % of the incident power either reflects back or is absorbed by the load of the adjacent antenna element. That means, although the  $Z_{in}^*$  case can be immune from phase variation of input signals at the very close element spacing, it is not a good solution in the desire of high radiation efficiency.

TABLE 3.4 COMPARISON ANALYSIS TABLE FOR THREE TERMINATION NETWORKS

Termination Type	First Crossing Point	EVRC	EVRE
50-Ohm Case	$0.4 \lambda$	0.33	0.9
$Z_{11}^*$ Case	$0.4 \lambda$	0.27	0.93
$Z_{in}^*$ Case	$0.1 \lambda$	0.68	0.53

## Chapter 4

# New Spatial Correlation Formulations under Arbitrary AoA Scenarios

Signal fading due to multipath is the dominant impairment in mobile radio systems. To overcome this problem multiple antennas are employed to provide diversity. The performance of antenna arrays is evaluated by the spatial correlation between antennas. In this chapter, we will discuss antenna spatial correlation including AoA distributions of the spatial channel and how mutual coupling affect this parameter. We first introduce the 2-D approximate spatial correlation formulation and our proposed approximate spatial correlation formulation under arbitrary AoA scenarios in Section 4.1. In Section 4.2, we further combine our proposed formulation with the 2-D and 3-D spatial correlations taking antenna mutual coupling effect into consideration in the parameterized manner as presented in [19] and [20], respectively. The proposed antenna spatial correlation formulations not only reduce time complexity but also maintain good accuracy in correlation calculation. Furthermore, all the simulation results are provided using the setup like Figure 3.1 in Chapter 3 as the benchmark.

## 4.1 2-D Approximate Spatial Correlation Formulation under Arbitrary AoA Scenarios

### 4.1.1 Spatial Correlation under Small Angular Spread AoA Scenarios

A channel model that simultaneously characterizes the AoAs of multipath components is



called the spatial channel model and different phi-plane AoA PDFs have been proposed in [21]. Spatial correlation which incorporate AoA PDF at receiving end will show the characteristics of channel and antenna array. In [12], the author presented the approximate spatial correlation which is suitable for small angular-spread AoA distribution. If a signal of interest arriving at an array can be described by the summation of plane waves arriving from angles with AoA distribution  $p_\phi(\Phi)$ , then the spatial correlation between two points a distance  $d$  apart can be determined as [7]

$$\rho(d) = \int_{-\pi}^{\pi} \exp(j2\pi \frac{d}{\lambda} \sin(\phi)) p_\phi(\phi) d\phi \quad (4.1)$$

where  $\Phi$  is defined relative to the normal,  $\lambda$  is the wavelength and  $p_\phi(\Phi)$  is the azimuth angular PDF. If the angular energy is a raised-cosine distribution, AoA distribution  $p_\phi(\Phi)$  can be represented as

$$P_\phi(\phi) = \begin{cases} \frac{1}{2\Delta_s} \left\{ 1 + \cos \left[ \frac{\pi(\phi - \phi_0)}{\Delta_s} \right] \right\}, & \text{for } -\Delta_s \leq \phi - \phi_0 \leq \Delta_s \\ 0, & \text{for } \phi - \phi_0 > \Delta_s \text{ or } \phi - \phi_0 < -\Delta_s \end{cases} \quad (4.2)$$

where  $2\Delta_s$  is the range of angles about the mean angle  $\Phi_0$ . Another common assumption for angular energy distribution is a Laplacian distribution and it is defined as

$$P_\phi(\phi) = \frac{1}{\sqrt{2}\sigma} \exp\left(-\frac{\sqrt{2}|\phi - \phi_0|}{\sigma}\right) \quad (4.3)$$

where  $\sigma$  is the standard deviation of the distribution and  $\Phi_0$  is the mean angle of AoA.

Substituting equation (4.2) into equation (4.1) and making a change of variables, the spatial correlation is given by

$$\rho(d) = \frac{1}{2} \int_{-1}^1 \exp\left\{j2\pi \frac{d}{\lambda} \sin(\Delta_s z + \phi_0)\right\} \{1 + \cos(\pi z)\} dz \quad (4.4)$$

Under the assumption of small  $\Delta_s Z$  over the integration range, equation (4.4) can be

approximated as

$$\rho(d) = \frac{1}{2} \exp(j2\pi \frac{d}{\lambda} \sin \phi_0) \left\{ 2 \sin c(2 \frac{d}{\lambda} \Delta_s \cos \phi_0) + \sin c(2 \frac{d}{\lambda} \Delta_s \cos \phi_0 - 1) + \sin c(2 \frac{d}{\lambda} \Delta_s \cos \phi_0 + 1) \right\} \quad (4.5)$$

Similarly substitute equation (4.3) into equation (4.1) and the spatial correlation based on Laplacian energy distribution can be approximated as

$$\rho(d) = \exp(j2\pi \frac{d}{\lambda} \sin \phi_0) \left\{ \frac{2}{2 + (\frac{2\pi d}{\lambda} \cos \phi_0 \sigma)^2} \right\} \quad (4.6)$$

equation (4.5) and equation (4.6) have provided a simple formula for spatial correlation calculation. The advantage of equation (4.5) and equation (4.6) is that they have reduced the computation time where the calculation of the spatial correlation originally relies on numerical integration or infinite series expansion. However, based on the discussion as shown in [12], equation (4.5) and equation (4.6) cannot approximate well when the angular spread of AoA distribution becomes larger. It is therefore not practical because the angular spread of the AoA distribution may become larger in the multiple scattering-rich environment, especially in the indoor environment. As a result, we will further propose the spatial correlation formulation which is suitable for large angular-spread AoA distribution and even arbitrary AoA scenarios.

### 4.1.2 Spatial Correlation under Arbitrary AoA Scenarios

The approximate spatial correlation formulations are presented based on raised-cosine and Laplacian distributions which are suitable for small angular spread AoA distribution in the previous section. However, the approximation may be distorted when the angular spread

becomes large and that is the reason why we would like to propose a good approximate spatial correlation formulation under large angular spread AoA scenarios.

Uniform distribution is suitable to describe large angular spread AoA in multiple scattering rich environments and its probability density function is presented as

$$p_{\phi}(\phi) = \frac{1}{2\Delta} \quad \phi_0 - \Delta \leq \phi \leq \phi_0 + \Delta \quad (4.7)$$

,where  $\Phi_0$  is the mean of the given uniform distribution and  $2\Delta$  is the range of angles referred to  $\Phi_0$ . If  $2\Delta$  is equal to  $2\pi$ , the spatial correlation has a closed form and is well-known as the Bessel function; however, for the case that  $2\Delta$  is smaller than  $2\pi$ , the spatial correlation is not a closed form formula and thus the time-consuming numerical integration is needed. Based on equation (4.2) and equation (4.3), we further propose two new approximate AoA distributions for the uniform distribution and they are shown below

$$P_{\phi}(\phi) = \begin{cases} \frac{1}{2N\Delta_s} \sum_{n=1}^N \left\{ 1 + \cos \left[ \frac{\pi(\phi - \phi_n)}{\Delta_s} \right] \right\}, & \text{for } -\Delta_s \leq \phi - \phi_n \leq \Delta_s \\ 0, & \text{for } \phi - \phi_n > \Delta_s \text{ or } \phi - \phi_n < -\Delta_s \end{cases} \quad (4.8)$$

and

$$P_{\phi}(\phi) = \frac{1}{\sqrt{2}N\sigma} \sum_{n=1}^N \exp \left( -\frac{\sqrt{2}|\phi - \phi_n|}{\sigma} \right) \quad (4.9)$$

where  $N$  is the number of sampling raised-cosine and Laplacian distribution,  $\Phi_n$  is the  $n$ -th sampling mean AoA.  $2\Delta_s$  is the range of angle about sampling mean AoA  $\Phi_n$  of raised-cosine distribution and  $\sigma$  is the AoA angular spread of Laplacian distribution. Both these approximate AoA distributions use the combination of many small angular spread raised-cosine and Laplacian distributions to fit a given large angular spread uniform distribution as shown in Figure 4.1(a), respectively. Since both raised-cosine and Laplacian distributions are general distributions to describe small angular spread AoA scenario and each

of them has a generalized approximate formulation like equation (4.5) and equation (4.6), they are suitable candidates as a fitting function of uniform distribution.

By substituting equation (4.8) and equation (4.9) into equation (4.1), we represent these two spatial correlations as

$$\rho(d) = \frac{1}{2N\Delta_s} \sum_{n=1}^N \int_{-\pi}^{\pi} \exp(j2\pi \frac{d}{\lambda} \sin(\phi)) \left\{ 1 + \cos \left[ \frac{\pi(\phi - \phi_n)}{\Delta_s} \right] \right\} d\phi \quad (4.10)$$

and

$$\rho(d) = \frac{1}{\sqrt{2}N\sigma} \sum_{n=1}^N \int_{-\pi}^{\pi} \exp(j2\pi \frac{d}{\lambda} \sin(\phi)) \exp \left( -\frac{\sqrt{2}|\phi - \phi_n|}{\sigma} \right) d\phi \quad (4.11)$$

Using the small angular-spread approximate spatial correlation as shown in equation (4.5) and equation (4.6), we may finally respectively represent both of the spatial correlations as

$$\rho(d) = \frac{1}{2N} \sum_{n=1}^N \exp(j2\pi \frac{d}{\lambda} \sin \phi_n) \left\{ 2 \operatorname{sinc} \left( 2 \frac{d}{\lambda} \Delta_s \cos \phi_n \right) + \operatorname{sinc} \left( 2 \frac{d}{\lambda} \Delta_s \cos \phi_n - 1 \right) + \operatorname{sinc} \left( 2 \frac{d}{\lambda} \Delta_s \cos \phi_n + 1 \right) \right\} \quad (4.12)$$

and

$$\rho(d) = \frac{1}{N} \sum_{n=1}^N \exp(j2\pi \frac{d}{\lambda} \sin \phi_n) \left\{ \frac{2}{2 + \left( \frac{2\pi d}{\lambda} \cos \phi_n \sigma \right)^2} \right\} \quad (4.13)$$

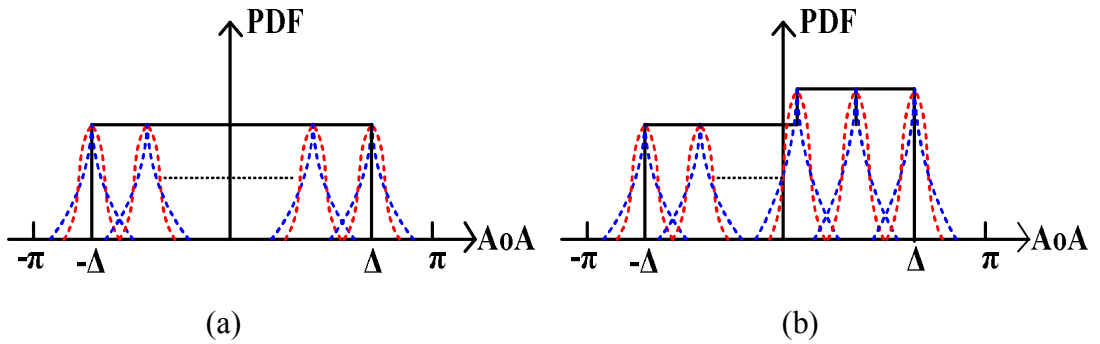


Figure 4.1 AoA distribution of (a) uniform distribution over  $-\Delta$  and  $\Delta$  and (b)

uniform-like distribution. The red dashed line and blue dashed line are the distribution curves of raised-cosine and Laplacian distributions, respectively.

The advantage of this approximation is it can be extended to arbitrary AoA scenarios as shown in Figure 4.1(b) as an example. For an AoA distribution which is very complex or cannot be described by a mathematical formula easily, the discretized summation is needed for correlation evaluation. The two approximate formulations we propose only samples specific mean AoAs over the distribution. Computation time of correlation calculation can thus be saved using these two proposed approximate formulations. The weighting coefficients of the sampling raised-cosine or Laplacian distributions may not equal  $1/N$  and should be modified according to the AoA scenario. Equation (4.12) and equation (4.13) should be modified as below

$$\rho(d) = \frac{1}{2N} \sum_{n=1}^N \alpha_n \exp(j2\pi \frac{d}{\lambda} \sin \phi_n) \left\{ 2 \operatorname{sinc}\left(2 \frac{d}{\lambda} \Delta_s \cos \phi_n\right) + \operatorname{sinc}\left(2 \frac{d}{\lambda} \Delta_s \cos \phi_n - 1\right) + \operatorname{sinc}\left(2 \frac{d}{\lambda} \Delta_s \cos \phi_n + 1\right) \right\} \quad (4.14)$$

and

$$\rho(d) = \frac{1}{N} \sum_{n=1}^N \beta_n \exp(j2\pi \frac{d}{\lambda} \sin \phi_n) \left\{ \frac{2}{2 + \left(\frac{2\pi d}{\lambda} \cos \phi_n \sigma\right)^2} \right\} \quad (4.15)$$

,where  $\alpha_n$  and  $\beta_n$  are the weighting coefficients which may modified according to the corresponding arbitrary AoA scenario.

### 4.1.3 Simulation Results and Discussions

We first show the performance of 2-D envelope correlation between two ideal sources by the conventional numerical integrating method, conventional discretized summation and our approximate formulations based on two different basis functions. The envelope correlation

can be represented as the absolute square of spatial correlation and it is shown below

$$\rho_{12}^{env} = |\rho(d)|^2 \quad (4.16)$$

, which is described as the receive power correlation coefficient on the two branches.

Simulation programs are written in MATLAB<sup>®</sup> and run on PC with an Intel<sup>®</sup> Pentium IV 3-GHz CPU. A uniformly-distributed AoA scenario over  $[-150^\circ, 150^\circ]$  with mean angle  $0^\circ$  is chosen as the benchmark to evaluate the envelope correlation. The computation result of the numerical integration is chosen as the closed-form solution and is regarded as the benchmark for accuracy comparison

The sampling small angular spread raised-cosine and Laplacian distributions sample their mean angles every  $10^\circ$  with  $5^\circ$  standard deviations for both our approximation schemes. Moreover, for raised-cosine AoA distribution as shown in equation (4.8), the relation between  $\Delta_s$  and its standard deviation  $\sigma$  is shown as

$$\sigma = \Delta_s \sqrt{\frac{1}{3} - \frac{2}{\pi^2}} \quad (4.17)$$

The correlations calculated by four different schemes in Figure 4.2 share similar curve trend with little variation. Numerical integration costs more time than the other two schemes as shown in Table 4.1; the main efficiency comparison is made between discretized summation and our two approximate formulations, namely equation (4.12) and equation (4.13). We find that the computation time of envelope correlation using equation (4.12) and equation (4.13) is reduced 51 % and 76% compared to that of discretized summation, respectively. We can also observe that the envelope correlation using equation (4.13) is faster than that using equation (4.12) and it is simply because there are fewer terms in equation (4.13) than in equation (4.12).

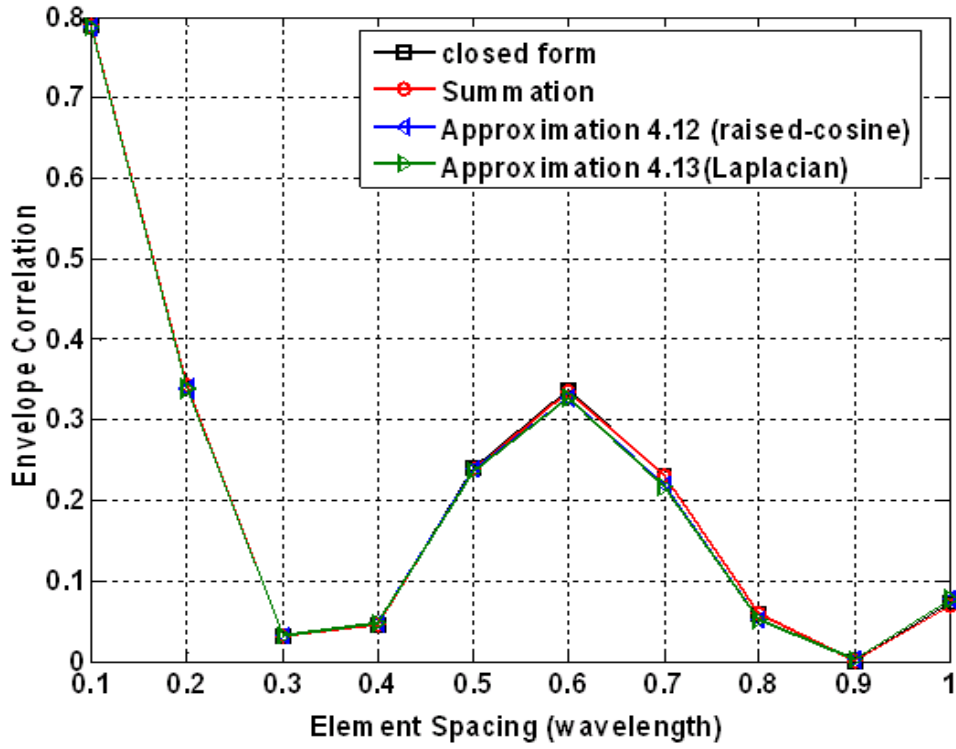


Figure 4.2 Envelope correlation of the given AoA scenario using different calculation schemes.

The accuracies of envelope correlation using equation (4.12) and equation (4.13) are the same under the same angular spread as shown in Table 4.2. The reason for this phenomenon is

discussed as below: It is known that  $\frac{1}{1-x}$  can be approximated by  $\sum_{n=0}^{\infty} x^n$  and  $\sin(x)$  can be

approximated by  $\sum_{n=0}^{\infty} \frac{(-1)^n x^{2n+1}}{(2n+1)!}$  where  $x = \frac{2\pi d}{\lambda} \sigma \cos \phi_n$ . Examining equation (4.12) and

equation (4.13) using Taylor series expansion, we can find these two formulations are almost the same and the approximate result is shown as

$$\rho(d) \approx \frac{1}{N} \sum_{n=1}^N \exp(j2\pi \frac{d}{\lambda} \sin \phi_n) \left\{ 1 - \frac{1}{2} \left( 2\pi \frac{d}{\lambda} \sigma \cos \phi_n \right)^2 \right\}. \text{The higher order terms of the}$$

Taylor series are omitted since we assume the angular spreads of the two AoA distributions are small ( $\sigma=5^\circ$ ). By this careful examination, we can know that equation (4.12) and equation

(4.13) are almost the same. As a result, the RMS errors of envelope correlation have the same values which match the results of Table 4.2. However, the calculation using these two approximate formulations still maintains good accuracy compared to numerical integrating method.

TABLE 4.1 EFFICIENCY COMPARISONS OF DIFFERENT SCHEMES IN FIGURE 4.2

Scheme	Computation time
Numerical Integration	0.250 sec.
Discretized Summation	0.063 sec.
Approximation 4.12 (raised-cosine)	0.031 sec.
Approximation 4.13 (Laplacian)	0.015 sec.

TABLE 4.2 ACCURACY COMPARISONS OF DIFFERENT SCHEMES IN FIGURE 4.2

Scheme	RMS Error
Approximation 4.12 (raised-cosine)	0.006
Approximation 4.13 (Laplacian)	0.006

## 4.2 Spatial Correlation Formulation Incorporating Antenna Mutual Coupling

### 4.2.1 2-D Formulation Derivation Incorporating Antenna



## Mutual Coupling

In Section 4.1, we have introduced our proposed approximate spatial correlation formulation under arbitrary AoA scenarios and it is shown that the computation time can be greatly reduced. Besides AoA distribution, the characteristics of multiple antennas also play an important role in the spatial correlation. One of the antenna characteristics like mutual coupling effect is considered an important factor in multiple antennas technology. To apply multiple antennas technology into devices of limited spacing results in high mutual coupling effect and directly impact spatial correlation. In [19], the authors derived an analytical expression for both the mean received power of each antenna and the spatial correlation between antennas with antenna mutual coupling under small angular spread AoA distribution. We want to combine our proposed approximate antenna spatial correlations with the analytical spatial correlation expression which is proposed in [19] in order to reach a more efficient calculation of the antenna spatial correlation under large angular spread AoA scenario.

Based on the equivalent circuit network model for multi-antenna array in [22], the extension version with incoming waves and load impedances are shown in Figure 4.3, where  $Z_{L1}, \dots, Z_{LN}$  are load impedances and  $Z_{A1}, \dots, Z_{AN}$  are antenna impedances. The incoming waves impinged on the array are equivalent to  $N$  outside sources  $V_{S1}, \dots, V_{SN}$  connected to the array elements, respectively. For closely spaced elements, mutual coupling needs to be considered and can be achieved by introducing a mutual coupling matrix. Using circuit theory the coupling matrix is given by

$$\mathbf{C} = (\mathbf{z}_L + \mathbf{z}_A)(\mathbf{Z}_L + \mathbf{Z})^{-1} \quad (4.18)$$

where  $z_L$  and  $z_A$  are the load impedance and antenna self impedance, and  $\mathbf{Z}_L$  and  $\mathbf{Z}$  are the load impedance matrix and antenna impedance matrix respectively. One thing which should

be mentioned is equation (4.18) is under the assumption that the multiple antenna systems is composed of identical antenna elements and terminated with the same load impedances.

For a dual antenna system, the coupling matrix is defined as

$$\mathbf{C} = \begin{bmatrix} a & b \\ b & a \end{bmatrix} \quad (4.19)$$

where  $a$  and  $b$  are called self coupling coefficient and mutual coupling coefficient respectively.

Consider there is no mutual coupling for the dual antenna system, and the received signal vector is given by

$$V^{nc}(\phi) = \begin{bmatrix} g_1(\phi) e^{-j\frac{\tau}{2}} & g_2(\phi) e^{j\frac{\tau}{2}} \end{bmatrix} \quad (4.20)$$

where  $g_x(\Phi)$  ( $x=1, 2$ ) is the radiation pattern of the  $x$ -th element without mutual coupling,  $\tau=2\pi d \sin(\Phi)/\lambda$  is the delay between two neighboring elements,  $d$  is the element spacing,  $\lambda$  is the wavelength and  $\Phi$  is the AoA. If taking mutual coupling into account, we may get the received signal vector as

$$V^c(\phi) = \mathbf{C} \cdot V^{nc}(\phi) = \begin{bmatrix} ag_1(\phi) e^{-j\frac{\tau}{2}} + bg_2(\phi) e^{j\frac{\tau}{2}} \\ ag_2(\phi) e^{j\frac{\tau}{2}} + ag_1(\phi) e^{-j\frac{\tau}{2}} \end{bmatrix} = \begin{bmatrix} V_1^c(\phi) \\ V_2^c(\phi) \end{bmatrix} \quad (4.21)$$

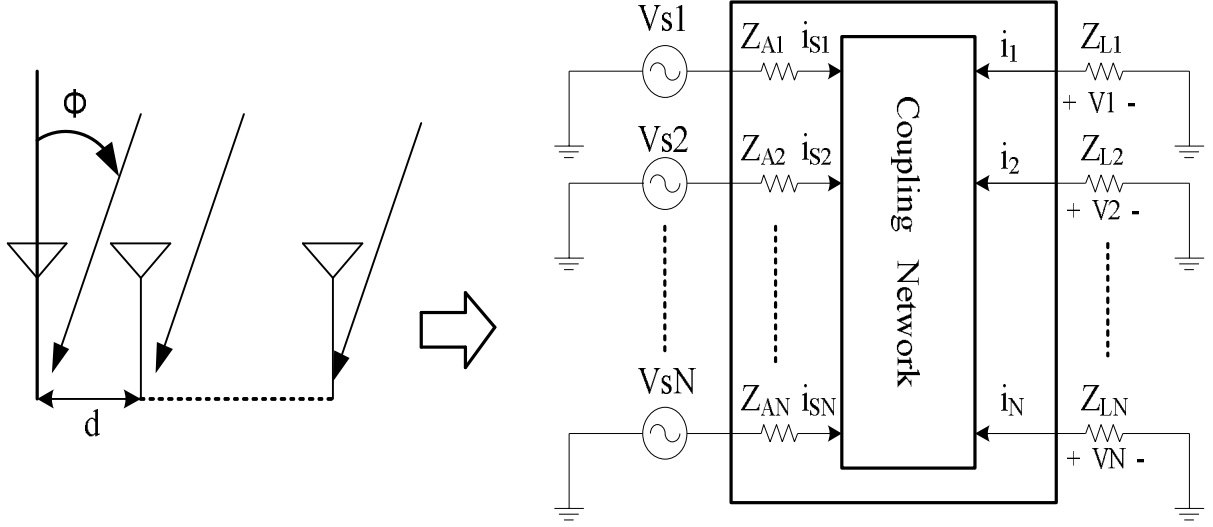


Figure 4.3 Equivalent circuit of the multiple antenna system for receiving mode.

Given the azimuth AoA distribution  $p(\Phi)$ , the spatial correlation is therefore shown as

$$\rho_{12}^c = \frac{1}{\sqrt{P_1 P_2}} \int_{\phi} V_1^c(\phi) V_2^{c*}(\phi) p(\phi) d\phi \quad (4.22)$$

where

$$P_i = \int_{\phi} |V_i^c(\phi)|^2 p(\phi) d\phi \quad (4.23)$$

For omnidirectional element patterns ( $g_1(\Phi) = g_2(\Phi) = 1$ ) without mutual coupling, the spatial correlation is denoted as

$$\rho_{12}^{omn-nc} = \int_{\phi} \exp\left\{j2\pi \frac{d}{\lambda} \sin \phi\right\} p(\phi) d\phi = R_{real} + jR_{imag} \quad (4.24)$$

After the cumbersome deduction, the analytical correlation coefficient expression taking mutual coupling effect into consideration is represented as

$$\rho_{12}^{omn-c} = \frac{\left[2 \operatorname{Re}(c) + (1 + |c|^2) \cdot R_{real} + j(1 - |c|^2) \cdot R_{imag}\right]}{\sqrt{\left[1 + |c|^2 + 2 \operatorname{Re}(c) \cdot R_{real}\right]^2 - 4 \left[\operatorname{Im}(c) \cdot R_{imag}\right]^2}} \quad (4.25)$$

where  $c$  is the ratio of mutual coupling coefficient  $b$  to self coupling coefficient  $a$ .

Equation (4.25) separates the element factors, including antenna mutual coupling and AoA scenarios, so that the spatial correlation can be dissected for a more detailed analysis. Moreover, another advantage is that we can combine our proposed approximate antenna spatial correlation with equation (4.25). That is to say,  $R_{\text{real}}$  and  $R_{\text{imag}}$  can be calculated in our two proposed approximate formulations and substitute them into equation (4.25) to achieve a more efficient calculation of the antenna spatial correlation.

## 4.2.2 3-D Formulation Derivation Incorporating Antenna Mutual Coupling

Various definitions of antenna spatial correlation have been introduced in Chapter 2. However, the above definitions have their limited merits. Equation (2.15) is derived under the assumption of the isotropic AoA distribution, but AoA distribution should vary with the environmental condition. Equation (4.25) in the previous section is another proposal which considers the 2-D antenna pattern and AoA. But the whole antenna pattern should be 3-D case and the polarization is not included in the definition. equation (2.17) is the most general definition of the spatial correlation; however, compared to equation (2.15) and equation (4.25) which both represent spatial correlation in parameterized manner, equation (2.17) is more computationally complex because 3-D antenna patterns need to be computed individually. In [20] a parameterized antenna spatial correlation formulation is proposed which takes individual 3-D antenna pattern and AoA scenarios into consideration. In this section we will briefly introduced this 3-D parameterized antenna spatial correlation formulation and show how it combines with our proposed approximate methods to reach a more efficient calculation.

Consider two antennas without mutual coupling, and the 3-D received signal vector of the two-element array can be shown as

$$V^{nc} = \begin{bmatrix} g_{\theta,1}(\theta,\phi)\hat{\theta} + g_{\phi,1}(\theta,\phi)\hat{\phi} \\ \left( g_{\theta,2}(\theta,\phi)\hat{\theta} + g_{\phi,2}(\theta,\phi)\hat{\phi} \right) \cdot e^{j\tau} \end{bmatrix} \quad (4.26)$$

where  $g_{\theta}(\theta,\Phi)$  and  $g_{\phi}(\theta,\Phi)$  are the isolated antenna pattern in theta and phi polarization, and  $\tau=2\pi d\sin(\Phi)\sin(\theta)/\lambda$  is the three-dimensional signal phase difference between two antenna elements. We further incorporate equation (4.19) into equation (4.26), and the signal vector can be rewritten as

$$\begin{aligned} V^c &= \begin{bmatrix} ag_{\theta,1}(\theta,\phi)e^{-j\tau/2} + bg_{\theta,2}(\theta,\phi)e^{j\tau/2} \\ ag_{\theta,2}(\theta,\phi)e^{j\tau/2} + bg_{\theta,1}(\theta,\phi)e^{-j\tau/2} \end{bmatrix} \hat{\theta} \\ &+ \begin{bmatrix} ag_{\phi,1}(\theta,\phi)e^{-j\tau/2} + bg_{\phi,2}(\theta,\phi)e^{j\tau/2} \\ ag_{\phi,2}(\theta,\phi)e^{j\tau/2} + bg_{\phi,1}(\theta,\phi)e^{-j\tau/2} \end{bmatrix} \hat{\phi} \\ &= \begin{bmatrix} C_{\theta,1}(\theta,\phi) \\ C_{\theta,2}(\theta,\phi) \end{bmatrix} \hat{\theta} + \begin{bmatrix} C_{\phi,1}(\theta,\phi) \\ C_{\phi,2}(\theta,\phi) \end{bmatrix} \hat{\phi} = \begin{bmatrix} C_1(\theta,\phi) \\ C_2(\theta,\phi) \end{bmatrix} \end{aligned} \quad (4.27)$$

where a and b are the self-coupling and mutual coupling coefficient respectively. The spatial correlation between two antennas is then defined as

$$\rho_{12} = \frac{R_{12}}{\sqrt{P_1 P_2}} = \frac{1}{\sqrt{P_1 P_2}} \int_0^{2\pi} \int_0^{\pi} C_1(\theta,\phi) C_2^*(\theta,\phi) p_{\theta,\phi}(\theta,\phi) \sin\theta d\phi d\theta \quad (4.28)$$

where  $p_{\theta,\phi}(\theta,\Phi)$  is the 3-D AoA distribution in theta and phi polarization, and  $R_{12}$  and  $P_i$  ( $i=1, 2$ ) are the covariance and the mean received power of the  $i$ -th antenna, where  $P_i$  is defined as

$$P_i = \int_0^{2\pi} \int_0^{\pi} |C_i(\theta,\phi)|^2 p_{\theta,\phi}(\theta,\phi) \sin\theta d\phi d\theta \quad (4.29)$$

After a cumbersome derivation, the 3-D analytical correlation coefficient expression taking mutual coupling effect into consideration is represented as

$$\rho_{12}^c = \frac{2\text{Re}(c)(A_\theta + A_\phi) + (1 + |c|^2)(R_{\text{real},\phi} + R_{\text{real},\theta})}{\sqrt{\left[\left(1 + |c|^2\right)(A_\theta + A_\phi) + 2\text{Re}(c)(R_{\text{real},\phi} + R_{\text{real},\theta})\right]^2 - 4\left[\text{Im}(c)(R_{\text{img},\phi} + R_{\text{img},\theta})\right]^2}} + \frac{j(1 - |c|^2)(R_{\text{img},\phi} + R_{\text{img},\theta})}{\sqrt{\left[\left(1 + |c|^2\right)(A_\theta + A_\phi) + 2\text{Re}(c)(R_{\text{real},\phi} + R_{\text{real},\theta})\right]^2 - 4\left[\text{Im}(c)(R_{\text{img},\phi} + R_{\text{img},\theta})\right]^2}} \quad (4.30)$$

where the lowercase  $c$  is the coupling ratio whose value is equal to  $b/a$ .  $A$  is the mean received power,  $R_{\text{real}}$  and  $R_{\text{imag}}$  are the real and imaginary part of covariance for single antenna pattern without mutual coupling, and the subscript  $\theta$  and  $\Phi$  are the value in theta and phi polarization respectively.  $A$ ,  $R_{\text{real}}$  and  $R_{\text{imag}}$  are listed below

$$A = \int_0^{2\pi} \int_0^\pi |g(\phi, \theta)|^2 p(\phi, \theta) \sin \theta d\theta d\phi \quad (4.31)$$

$$R_{\text{real}} = \text{Re} \left( \int_0^{2\pi} \int_0^\pi g_1(\phi, \theta) g_2^*(\phi, \theta) p(\phi, \theta) \sin \theta d\theta d\phi \right) \quad (4.32)$$

$$R_{\text{imag}} = \text{Im} \left( \int_0^{2\pi} \int_0^\pi g_1(\phi, \theta) g_2^*(\phi, \theta) p(\phi, \theta) \sin \theta d\theta d\phi \right) \quad (4.33)$$

What should be mentioned is the polarization of AoA distribution is defined as

$$p_\theta(\phi, \theta) = \frac{1}{1 + XPR} \cdot p_{\theta,\phi}(\phi, \theta) \quad (4.34)$$

$$p_\phi(\phi, \theta) = \frac{XPR}{1 + XPR} \cdot p_{\theta,\phi}(\phi, \theta) \quad (4.35)$$

where  $XPR$  denotes the cross polarization ratio and in the later simulation setup we regard  $\theta$ -polarization as the main polarization and  $\Phi$ -polarization as the cross polarization.

One advantage of equation (4.30) is that we only have to obtain an isolated 3-D antenna pattern and the coupling matrix to compute the antenna spatial correlation. The resource-consuming process which records the individual coupling antenna pattern can be

avoided. The other advantage of equation (4.30) is that it can be combined with our proposed approximate correlation formulations like equation (4.14) and equation (4.15) to perform a more efficient correlation calculation.

### 4.2.3 Simulation Results and Discussions

According to the discussions in [20], equation (4.25) and equation (4.30) are both good candidates for the calculation of 2-D and 3-D antenna spatial correlations incorporating antenna mutual coupling, respectively. As a result, we will perform several calculation schemes including Numerical integration, Discretized summation and our two proposed approximation methods to calculate the envelope correlations using equation (4.25) and equation (4.30). Numerical integration method is chosen as the closed-form solution for the benchmark of accuracy comparison. Moreover, the HFSS simulation setup of the coupled dipole pair is the same as shown in Figure 3.1 in Chapter 3. The port impedance set to be 50 Ohm and the Z-parameter is extracted from this setup, while simulation programs are written in MATLAB<sup>®</sup> and run on PC with an Intel<sup>®</sup> Pentium IV 3-GHz CPU.

First we evaluate 2-D spatial correlation with antenna mutual coupling effect using equation (4.25). A uniformly-distributed AoA scenario over  $[-150^{\circ}, 150^{\circ}]$  is chosen as the benchmark to evaluate the spatial correlation. The sampling small angular spread raised-cosine and Laplacian AoA distributions sample their mean angles every  $10^{\circ}$  with  $5^{\circ}$  standard deviation for both our approximation schemes and they will calculate  $R_{\text{real}}$  and  $R_{\text{imag}}$  in equation (4.25). Moreover, the 2-D envelope correlation taking mutual coupling effect into account is defined as  $|\rho_{12}^{\text{omn-c}}|^2$ . Figure 4.4 shows the envelope correlations both with and without mutual coupling effect by performing different calculation schemes in equation (4.25).

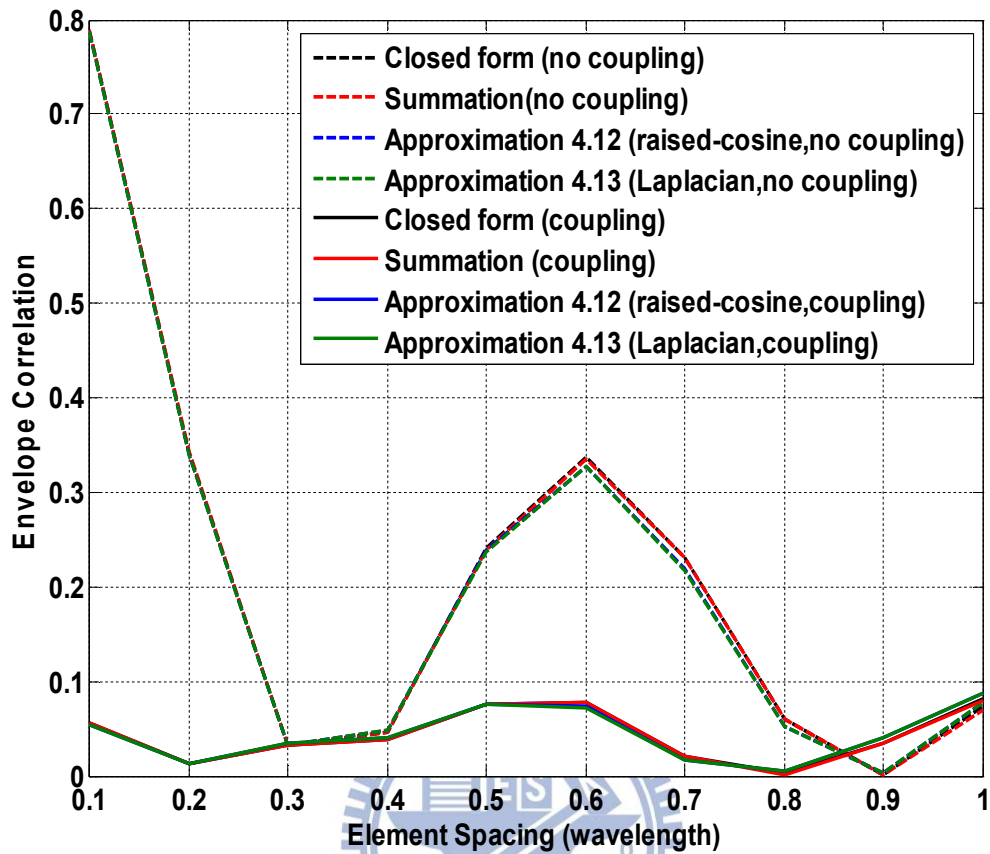


Figure 4.4 2-D Envelope correlation of the given AoA scenario with and without mutual coupling effect using different calculation schemes

TABLE 4.3 ACCURACY COMPARISONS OF DIFFERENT SCHEMES IN FIGURE 4.4  
(COUPLING)

Scheme	RMS Error
Approximation 4.12 (raised-cosine)	0.0035
Approximation 4.13 (Laplacian)	0.0035



From the perspective of physical meaning in Figure 4.4, the mutual coupling effect can effectively reduce the correlation at close antenna spacings just as the conclusion which [19] suggested. For accuracy comparison as shown in Table 4.3, we can find that the two approximation schemes have the same RMS errors compared to Numerical integration method again. The reason has been discussed in the previous section. However, the two proposed approximation methods still maintain good accuracy compared to Numerical integration method.

We further evaluate 3-D envelope correlation with antenna mutual coupling effect between two 2.45GHz dipole antennas using equation (4.30), while the 3-D envelope correlation is defined as  $|\rho_{12}^c|^2$ . Different calculation schemes will also be performed in this parameterized spatial correlation formulation. One thing should be mentioned is that for closed-form Numerical integration method, we choose theoretical  $\lambda/2$  dipole pattern function for calculation. The 3-D AoA scenario for this case study in Figure 4.5 is a 3-D normalized distribution which is an arbitrarily-chosen Rayleigh-Gaussian-distributed PDF in phi plane and a  $5^\circ$  standard deviation Gaussian distribution with mean  $90^\circ$  in theta plane, this scenario is practical in the indoor NLOS channel and similar to the scenario measured in [23]. XPR is assumed to be 0 for this case. Moreover, we can exploit the modified approximate formulations (equation (4.14) and equation (4.15)) in phi plane to approximate the arbitrary-chosen AoA distribution by using the same antenna setup as 2-D case, while in theta plane AoA distribution we choose discretized summation in order to maintain good accuracy.

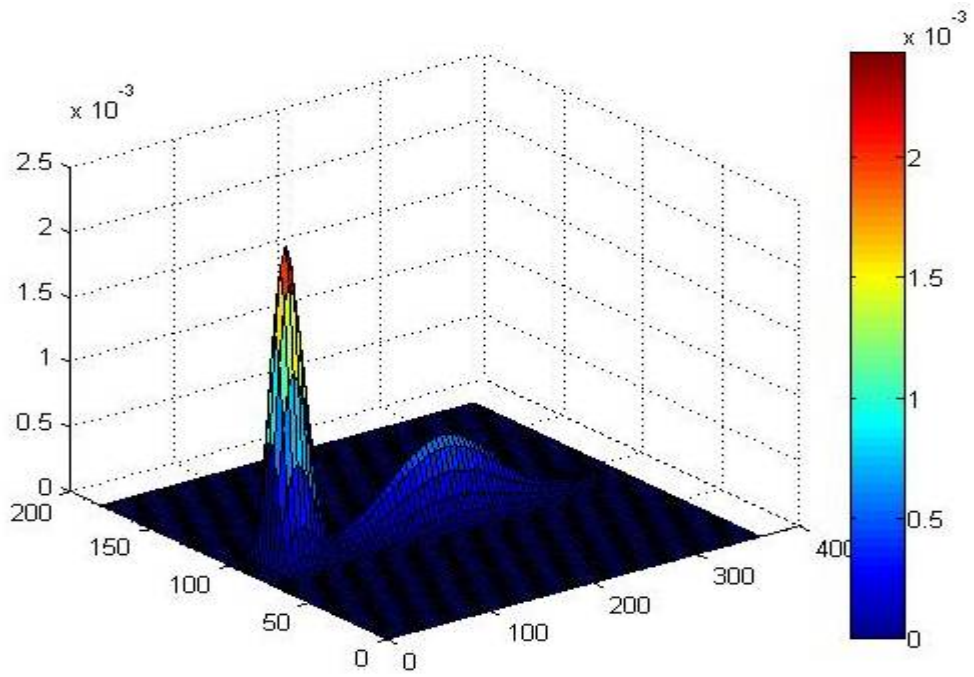


Figure 4.5 The 3-D AoA distribution in Section 4.2.3

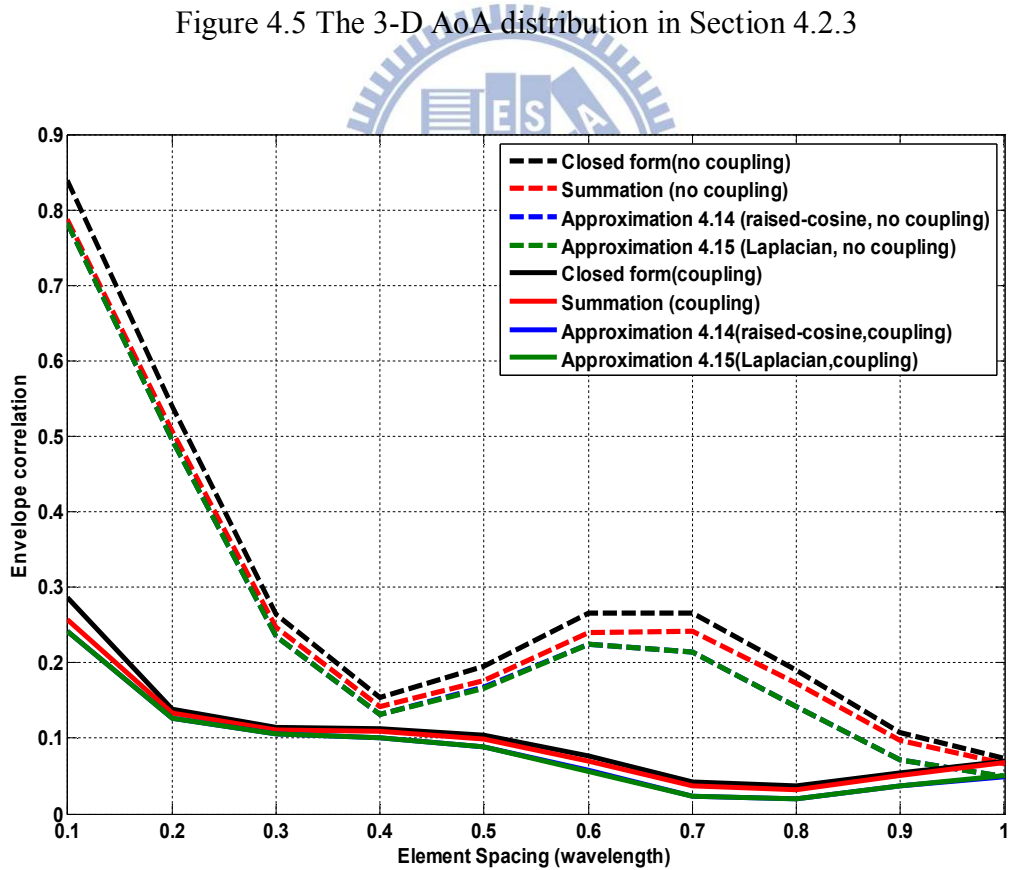


Figure 4.6 3-D Envelope correlation of the given AoA scenario with and without mutual coupling effect using different calculation schemes

TABLE 4.4 EFFICIENCY COMPARISONS OF DIFFERENT SCHEMES IN FIGURE 4.6

Scheme	Computation time
Numerical Integration	21.8 sec.
Discretized Summation	4.5 sec.
Approximation 4.14 (raised-cosine)	3.2 sec.
Approximation 4.15 (Laplacian)	1.7 sec.

TABLE 4.5 ACCURACY COMPARISONS OF DIFFERENT SCHEMES IN FIGURE 4.6

(COUPLING)

Scheme	RMS Error
Approximation 4.14 (raised-cosine)	0.012
Approximation 4.15 (Laplacian)	0.012

The computation results of the envelope correlation are shown in Figure 4.6. The efficiencies comparison for the four calculation schemes are shown in Table 4.4 and the accuracies comparison for our two proposed approximate correlations are shown in Table 4.5. We can observe that the computation times using two of our proposed approximate formulations are greatly reduced (more than 28 %) compared to conventional discretized summation method. Moreover, the accuracies still maintain good using our two proposed methods. For a given AoA distribution, antenna spatial correlation tends to decrease with some oscillation as element spacing increase. On the other hand, mutual coupling again reduce the antenna correlation at very close element spacing.

For MIMO operation, mobile devices such as PDA phone or smart phone may contain more than two antennas [24]. For this kind of antennas setup, spatial correlation matrix is used to describe the correlation values between different antenna pairs. By combining equation (4.14) and equation (4.15) with the equation (4.30), we can compute each entry in the correlation matrix more efficient and the computation time for the calculation of whole spatial correlation matrix can be significantly reduced.



# Chapter 5

## Conclusions

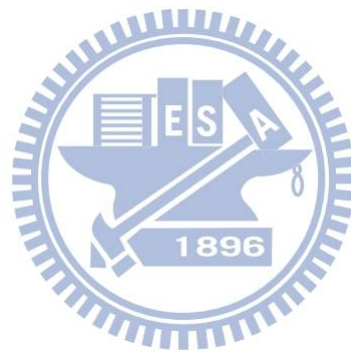
In this thesis, we focus on two new electromagnetic analysis strategies to evaluate the performance of multiple antenna systems. The first is an analysis strategy of radiation efficiency, and the others are two new antenna spatial correlation formulations. All the simulation results are provided using dipole antennas as the benchmark.

First, the discussion of analysis strategy utilizing EVD on reflection power matrix not only evaluate how the radiation efficiency change when the antenna ports excitation signals with different phases for dual antenna systems, but also provided a fast way to evaluate the minimum and maximum values of reflection coefficient or radiation efficiency and the corresponding input excitation signals when the number of antennas is more than two. This new analysis strategy is important when MIMO systems operate in transmitting mode. Furthermore, the investigation of how termination networks on radiation efficiency are also conducted based on dual dipoles system.

Secondly, the two new approximate spatial correlation formulations are further proposed which are suitable for arbitrary large angular spread AoA distribution, both for 2-D and 3-D AoA scenarios. These new approximate formulations are useful when MIMO systems operate in receiving mode. Such these formulations can be combined with 2-D and 3-D parameterized spatial correlation formulations taking antenna mutual coupling into consideration in order to perform a more efficient calculation under arbitrary large AoA scenario.

These two new electromagnetic strategies are offered as the gauges to evaluate the performances of multiple antenna systems. With the proposed analysis strategies, we can

make the design of multiple antenna systems more efficient and persuasive before physical hardware implementation.



# Reference

- [1] D. Gesbert et al., "From theory to practice: an overview of space-time coded MIMO wireless systems," *IEEE JSAC*, Apr., 2003.
- [2] W.L.Stutzman and G.A.Thiele, *Antenna Theory and Design*, John Wiley & Sons, New York, NY, 1998
- [3] J. Litva, K. Y. Lo and Titus, *Digital Beamforming in Wireless Communications*, Artech House, Norwood, MA, 1996.
- [4] R.Goossens and H.Rogier," Optimal beam forming in the presence of mutual coupling," *IEEE Communications and Vehicular Technology Symposium*, vol.1, pp. 13-18, 2006.
- [5] P. S. Kildal and K. Rosengren, "Electromagnetic analysis of effective and apparent diversity gain of two parallel dipoles," *IEEE Antennas and Wireless Propagation Letters*, vol. 2, 2003.
- [6] R. G. Vaughan and J. B. Andersen, "Antenna diversity in mobile communications," *IEEE Trans. Vehicular Technology*, vol. 36, no. 4, Nov., 1987.
- [7] W. C. Jakes, *Microwave Mobile Communications*, Wiley, NY, 1974.
- [8] R. H. Clarke, "A statistical theory of mobile radio reception," *Bell Syst. Tech. J.*, vol. 47, pp. 957-1000, 1969.
- [9] W. C. Y. Lee, "Effect of correlation between two mobile radio base-station antennas," *IEEE Trans. Communications*, pp. 1214-1223, Nov, 1973.
- [10] Y.-Z Wang, Z.-C Zhou and J. Wang, "Analysis of spatial fading correlation for different antenna array," *IEEE Wireless Communications and Networking Conference*, vol.2, pp. 700-704, 2004.
- [11] J.-A Tsai, R. M. Buehrer and B. D. Woerner," Spatial Fading Correlation Function of Circular Antenna Arrays With Laplacian Energy Distribution," *IEEE Communications*

*Letters*, vol.6, 2002.

- [12] R. M. Buehrer, "The impact of angular energy distribution on spatial correlation," *IEEE Vehicular Technology Conference*, vol. 2, pp. 24-28, 2002.
- [13] S. Blanch, J. Romeu, and I. Corbella, "Exact representation of antenna system diversity performance from input parameter description," *Electronics Letters*, vol. 39, no. 9, 2003.
- [14] C. Waldschmidt, and W. Wiesbeck, "Compact wide-band multimode antennas for MIMO and diversity," *IEEE Trans. Antennas and Propag.*, vol. 52, no. 8, 2004.
- [15] D. M. Pozar, *Microwave Engineering*, 3rd ed., Wiley, New York, NY, 2005.
- [16] C. Volmer, J. Weber, R. Stephan, K. Blau, and M. Hein, "An eigen-analysis of compact antenna arrays and its application to port decoupling," *IEEE Trans. Antennas Propag.*, vol. 56, no. 2, pp. 360-370, Feb. 2008.
- [17] M. Manteghi and Y. Rahmat-Samii, "Multiport characteristics of a wide-band cavity backed annular patch antenna for multipolarization operations," *IEEE Trans. Antennas and Propag.*, vol. 53, no. 1, Jan., 2005.
- [18] D. W. Browne, M. Manteghi, M. P. Fitz and Y. Rahmat-Samii, "Experiments with compact antenna arrays for MIMO radio communications," *IEEE Trans. Antennas and Propag.*, vol. 54, no. 11, Nov., 2006.
- [19] X. Li and Z. Nie, "Effect of mutual coupling on performance of MIMO wireless channels," *ICMMT 4<sup>th</sup> International Conference*, pp. 18-21, 2004.
- [20] 謝博全, 「新型態多天線系統綜合分析」, 國立交通大學, 碩士論文, 民國 96 年。
- [21] J. Fuhl, A. F. Molisch, and E. Bonek, "Unified channel model for mobile radio systems with smart antennas," *IEE Proc. Radar, Sonar Navigation*, vol. 145, no. 1, 1998.
- [22] I. J. Gupta and A. A. Ksienski, "Effect of mutual coupling on the performance of adaptive arrays," *IEEE Trans. Antennas and Propag.*, vol. AP-31, no. 5, 1983.
- [23] B. K. Lau, J. B. Andersen, G. Kristensson, and A. F. Molisch, "Impact of matching network on bandwidth of compact antenna arrays," *IEEE Trans. Antennas and Propag.*, vol. 54, no. 11, Nov., 2006.



- [24] K. L. Wong, C. H. Chang, B. Chen, and S. Yang, "Three-antenna MIMO system for WLAN operation in a PDA phone," *Microwave and Optical Technology Letters*, vol. 48, no. 7, pp. 1238-1242, 2006.

